Homeostatic Synaptic Plasticity of Miniature Excitatory Postsynaptic Currents in Mouse Cortical Cultures Requires Neuronal Rab3A

Andrew G. Koesters[1*], Mark M. Rich[2], and Kathrin L. Engisch[3]

[1]Department of Pharmacology, Physiology, and Neurobiology, University of Cincinnati College of Medicine, Cincinnati, OH 45267, USA
[2]Department of Neuroscience, Cell Biology and Physiology, Boonshoft School of Medicine, Wright State University, Dayton, OH 45345
[3]Department of Neuroscience, Cell Biology and Physiology, Boonshoft School of Medicine and the College of Science and Mathematics, Wright State University, Dayton, OH 45435

*Andrew G. Koesters –Corresponding author
Department of Pharmacology, Physiology, and Neurobiology, University of Cincinnati College of Medicine, Cincinnati, OH 45267, USA
koesteag@ucmail.uc.edu, ph 513-558-2819

Author contributions: A.G.K., K.L.E. and M.M.R. designed research; A.G.K. performed research; A.G.K. and K.L.E. analyzed data; A.G.K, K.L.E., and M.M.R. wrote the paper.

ORCID iDs: ; A.G.K, https://orcid.org/0000-0003-3281-188X; M.M.R., https://orcid.org/0000-0002-6956-5531; K.L.E., https://orcid.org/0000-0002-1058-5343

The authors have no competing interests.

Keywords: Homeostatic Synaptic Plasticity; Synaptic Scaling; mEPSCs; Rab3A; AMPA receptors

Acknowledgements: The authors thank E. Whitlock and H. Ghouse for their contributions to confocal image analyses. This work was partially supported by NINDS P01 NS057228, Tim Cope, PI, KE, PI project 4.

30 Abstract

31 Following prolonged activity blockade, amplitudes of miniature excitatory postsynaptic currents
32 (mEPSCs) increase, a form of plasticity termed "homeostatic synaptic plasticity." We previously
33 showed that a presynaptic protein, the small GTPase Rab3A, is required for full expression of
34 the increase in miniature endplate current amplitudes following prolonged blockade of action
35 potential activity at the mouse neuromuscular junction in vivo, where an increase in
36 postsynaptic receptors does not contribute (Wang et al., 2005; Wang et al., 2011). It is
37 unknown whether this form of Rab3A-dependent homeostatic plasticity at the neuromuscular
38 junction shares any characteristics with central synapses. We show here that homeostatic
39 synaptic plasticity of mEPSCs is impaired in mouse cortical neuron cultures prepared from
40 Rab3A$^{-/-}$ and mutant mice expressing a single point mutation of Rab3A, Rab3A Earlybird mice.
41 To determine if Rab3A is involved in the well-established homeostatic increase in postsynaptic
42 AMPA-type receptors (AMPARs), we performed a series of experiments in which
43 electrophysiological recordings of mEPSCs and confocal imaging of synaptic AMPAR
44 immunofluorescence were assessed within the same cultures. We found that the increase in
45 postsynaptic AMPAR levels in wild type cultures was more variable than that of mEPSC
46 amplitudes, which might be explained by a presynaptic contribution, but we cannot rule out
47 variability in the measurement. Finally, we demonstrate that Rab3A is acting in neurons
48 because only selective loss of Rab3A in neurons, not glia, disrupted the homeostatic increase in
49 mEPSC amplitudes. This is the first demonstration that a protein thought to function
50 presynaptically is required for homeostatic synaptic plasticity of quantal size in central neurons.

51

52

53 Introduction

54 One of the most studied phenomena triggered by prolonged activity blockade is the
55 increase in amplitudes of miniature excitatory postsynaptic currents (mEPSCs) in neurons. First
56 demonstrated in cultures of dissociated cortical neurons (Turrigiano et al., 1998) and spinal
57 cord neurons (O'Brien et al., 1998), the compensatory response to prolonged loss of activity has
58 been dubbed “homeostatic synaptic plasticity” (Turrigiano and Nelson, 2004; Pozo and Goda,
59 2010). These first two studies provided evidence that glutamate receptors were also increased
60 after prolonged inactivity, via an increased response to exogenously applied glutamate
61 (Turrigiano et al., 1998) and increased immunofluorescent labeling of GluA1 receptors at
62 synaptic sites (O'Brien et al., 1998). The accompanying increase in synaptic AMPA receptors has
63 been confirmed with immunofluorescence in multiple studies of hippocampal and cortical
64 cultures treated with TTX, including (Wierenga et al., 2005; Hou et al., 2008; Ibata et al., 2008;
65 Jakawich et al., 2010; Tatavarty et al., 2013; Xu and Pozzo-Miller, 2017; Dubes et al., 2022). It is
66 now well accepted that the homeostatic increase in mEPSC amplitudes in neurons is due to an
67 increase in postsynaptic AMPA receptors.

68 In our previous work, we found that a TTX cuff applied for 48 hrs around the sciatic
69 nerve in mice led to an increase in the amplitude of the miniature endplate currents (mEPCs)
70 recorded in tibialis anterior muscles. Surprisingly, and unlike at central synapses, we could find
71 no evidence that the acetylcholine receptors levels at the neuromuscular junction (NMJ) were
72 increased in the TTX-cuff treated mice (Wang et al., 2005). This result led us to search for
73 presynaptic molecules that might homeostatically regulate the presynaptic quantum. In

74 previous studies in chromaffin cells, we identified the small GTPase Rab3A, a presynaptic vesicle
75 protein, as a regulator of synaptic vesicle fusion pore opening (Wang et al., 2008), so we
76 examined whether deletion of Rab3A (Rab3A$^{-/-}$) might prevent homeostatic upregulation of
77 mEPC amplitude at the NMJ. The results were clear: the homeostatic increase in mEPC
78 amplitude induced by the TTX cuff was strongly reduced in the Rab3A$^{-/-}$ mouse, and was
79 completely abolished in the Earlybird mutant (Rab3A$^{Ebd/Ebd}$), which has a single point mutation
80 in Rab3A that causes a shift towards early awakening due to a shorter circadian period, that is
81 more dramatic than that of the Rab3A deletion mouse (Kapfhamer et al., 2002; Wang et al.,
82 2011). These results led us to conclude that the homeostatic increase in mEPC amplitude at the
83 NMJ is a presynaptic phenomenon.

84 It has remained somewhat of a mystery what the role of Rab3A is in synaptic
85 transmission. The Rab3A$^{-/-}$ mouse has minimal phenotypic abnormalities, with evoked synaptic
86 transmission and mEPSCs essentially normal in hippocampal slices (Geppert et al., 1994). At the
87 Rab3A$^{-/-}$ NMJ, reductions in evoked transmission were detected, but only under conditions of
88 reduced extracellular calcium (Coleman et al., 2007). There are some modest changes in short
89 term plasticity during repetitive stimulus trains, with increased depression observed in
90 response to moderate frequencies in hippocampal slices (Geppert et al., 1994) and at the
91 mammalian NMJ (Coleman and Bykhovskaia, 2009), but increased facilitation in response to
92 high frequency stimulation at the mammalian NMJ (Coleman and Bykhovskaia, 2010). The most
93 dramatic effect of loss of Rab3A is the abolishment of a presynaptic form of long-term
94 potentiation (LTP) at the mossy fiber-CA3 synapse that is induced by 25 Hz stimulation in the
95 presence of NMDA blockers (Weisskopf et al., 1994; Castillo et al., 1997). Our result that

96 prolonged inactivity-induced plasticity of mEPC amplitude at the mammalian NMJ is disrupted
97 with loss of function of Rab3A further cements a role for Rab3A in activity-dependent plasticity
98 of synaptic strength. However, a crucial question that remains is whether the TTX-cuff induced
99 effect on the amplitude of the spontaneous synaptic current at the NMJ shares underlying
100 mechanisms with central synapses. We set out to answer this question for the more well-
101 studied phenomenon of homeostatic plasticity of mEPSCs in dissociated mouse cortical neurons
102 prepared from wild type, Rab3A$^{-/-}$ mice and Rab3a$^{Ebd/Ebd}$ mice treated with TTX for 48 hrs. We
103 show here that homeostatic synaptic plasticity of mEPSC amplitude was strongly reduced in
104 cultures from Rab3A$^{-/-}$ mice, and completely abolished in cultures from Rab3A$^{Ebd/Ebd}$ mice,
105 supporting a shared mechanism with the neuromuscular junction.

106

107

108 Results

109 We previously reported that mixed cultures of cortical neurons and glia prepared from
110 postnatal day 0-2 mouse pups responded to a block of action potential-mediated activity by a
111 48 hr TTX treatment with an increase in mEPSC amplitude (Hanes et al., 2020). Here, we asked
112 the question whether cortical cultures prepared from mice lacking the small GTPase Rab3A, or,
113 expressing a point mutation of Rab3A, Rab3A Earlybird, have an altered homeostatic plasticity
114 response to a prolonged loss of network activity. The Rab3A Earlybird mutation was discovered
115 in a mutagenesis screen in mice for genes involved in the rest-activity cycle (Kapfhamer et al.,
116 2002). In that study, the authors concluded that the Earlybird mutation was likely dominant-
117 negative, as the shift in circadian period was substantially more dramatic than that observed in
118 the Rab3A$^{-/-}$ mice. As described in the Introduction, the effects of loss of Rab3A have been
119 modest, so we included experiments using the Rab3A Earlybird mutant mice to see if there
120 would be a more robust phenotype, and in doing so, strengthen our conclusions based on the
121 Rab3A deletion mice. To obtain Rab3A$^{-/-}$ and Rab3A$^{Ebd/Ebd}$ homozygotes, we established two
122 mouse colonies of heterozygous breeders with cultures prepared from pups derived from a
123 final breeding pair of homozygotes. Although we backcrossed Rab3A$^{+/-}$ with Rab3A$^{+/Ebd}$ for 11
124 generations, clear differences in mEPSC amplitudes in untreated cortical cultures for the two
125 wild type strains (see below) and in calcium current amplitudes in adrenal chromaffin cells for
126 the two wild type strains (unpublished obs.) remained. Therefore, throughout this study there
127 are two Rab3A$^{+/+}$ or 'wild type' phenotypes.

128 We found that loss of Rab3A greatly impaired the homeostatic increase after activity
129 blockade. Example current traces of spontaneously occurring mEPSCs recorded from pyramidal

130 neurons in untreated (CON) 13-14 DIV cortical cultures and sister cultures treated with 500 nM
131 TTX for 48 hr prepared from wild type and Rab3A$^{-/-}$ mice in the Rab3A$^{+/-}$ colony are shown in
132 Figures 1A and B, respectively. Average mEPSC waveforms from the same recordings are shown
133 in Figures 1C and D. The mean mEPSC amplitudes for 30 control and 23 TTX-treated neurons
134 from Rab3A$^{+/+}$ cultures are displayed in the box and whisker plot in Figure 1E; after activity
135 blockade the average mEPSC amplitude increased from 13.9 ± 0.7 pA to 18.2 ± 0.9 pA. In
136 contrast, in cultures prepared from Rab3A$^{-/-}$ mice, the average mEPSC amplitude was not
137 significantly increased, for 25 untreated cells and 26 TTX-treated cells (Figure 1F, 13.6 ± 0.1 pA
138 vs. 14.3 ± 0.6 pA). We found that TTX treatment also resulted in an increase in mEPSC
139 frequency in cultures prepared from Rab3A$^{+/+}$ mice, as shown in Figure 1G (CON, 2.26 ± 0.37
140 sec^{-1}; TTX, 4.62 ± 0.74 sec^{-1}). This TTX-induced frequency increase was strongly reduced in
141 cultures from Rab3A$^{-/-}$ mice, but there were a few outliers with very high frequencies still
142 present after TTX treatment (Figure 1H, CON, 2.74 ± 0.49 sec^{-1}; TTX, 3.23 ± 0.93 sec^{-1}).
143 We next examined homeostatic plasticity in cultures prepared from wild type mice in
144 the Rab3A$^{+/Ebd}$ colony. Example current traces of mEPSCs, and average mEPSC waveforms, are
145 shown in Figures 2A and C, respectively, for cortical cultures prepared from wild type mice in
146 the Rab3A$^{+/Ebd}$ colony. Treatment with TTX for 48 hr led to a significant increase in the average
147 mEPSC amplitude of 23 TTX-treated cells when compared to 20 untreated cells (Figure 2E, CON,
148 11.0 ± 0.6 pA; TTX, 15.1 ± 1.2 pA). We note here that while the two wild type strains respond
149 very similarly to activity blockade, the mean mEPSC amplitude in untreated cultures was
150 different between the two strains, 13.9 ± 0.7 pA, wild type from Rab3A$^{+/-}$ colony; 11.0 ± 0.6 pA,

151 wild type from Rab3A$^{+/Ebd}$ colony, but this difference did not reach statistical significance in a
152 Tukey means comparison after a two-way ANOVA (p = 0.27).

153 We found a complete disruption of homeostatic plasticity in cortical cultures prepared
154 from Rab3A$^{Ebd/Ebd}$ mice, as can been seen in viewing example mEPSC traces and average mEPSC
155 waveforms (Figures 2B and D, respectively). The lack of TTX effect was confirmed in a
156 comparison of mEPSC amplitude means for 21 untreated and 22 TTX-treated cells (Figure 2F,
157 CON, 15.1 ± 1.0 pA vs. TTX, 14.6 ± 1.1 pA). There was a trend towards increased mEPSC
158 frequency in TTX-treated cultures from this wild type strain, but the difference was not as
159 robust as for the wild type cultures from Rab3A$^{+/-}$ colony, and did not reach statistical
160 significance (Figure 2G, CON, 1.15 ± 0.19 sec^{-1}; TTX, 2.54 ± 0.55 sec^{-1}). This trend was not
161 observed in neurons from cultures prepared from Rab3A$^{Ebd/Ebd}$ mice, likely due to an increase in
162 frequency in untreated cells—frequencies remained high in TTX-treated cells (Figure 2H, CON,
163 1.71 ± 0.41 sec^{-1}; TTX, 3.05 ± 0.80 sec^{-1}). Our results show that the homeostatic increase in
164 mEPSC amplitude after activity blockade is disrupted in both Rab3A$^{-/-}$ and the Rab3A$^{Ebd/Ebd}$
165 cortical neurons, strongly supporting a crucial role of functioning Rab3A in this process.

166 The disruption in homeostatic plasticity differs for Rab3A$^{-/-}$ and Rab3A$^{Ebd/Ebd}$. In the
167 Rab3A$^{-/-}$ data set, mEPSCs from untreated cultures were indistinguishable from mEPSCs from
168 Rab3A$^{+/+}$ untreated cultures, demonstrating loss of Rab3A has no impact on basal activity
169 mEPSC amplitudes. In the Rab3A$^{Ebd/Ebd}$ data set, mEPSC amplitudes from untreated cultures
170 were significantly larger than those of untreated cultures from wild type mice, as can be seen
171 comparing the CON values in Figures 2E and F (CON, Rab3A$^{+/+}$, 11.0 ± 0.7 pA, vs. CON,
172 Rab3A$^{Ebd/Ebd}$, 15.1 ± 1.0 pA, p = 0.04, Tukey means comparison after two-way ANOVA). The

173 increase in mEPSC amplitude in cultures from Rab3A$^{Ebd/Ebd}$ mice is consistent with the increase
174 in mEPC amplitude we observed at the Rab3A$^{Ebd/Ebd}$ NMJ (Wang et al., 2011).
175 The small GTPase Rab3A is generally thought to function presynaptically to regulate
176 synaptic vesicle trafficking, possibly in an activity-dependent manner (Castillo et al., 1997;
177 Lonart et al., 1998; Leenders et al., 2001; Schluter et al., 2006; Coleman and Bykhovskaia, 2009;
178 Tian et al., 2012). In contrast, homeostatic plasticity of mEPSC amplitude has been attributed to
179 an increase in postsynaptic receptors on the surface of the dendrite (O'Brien et al., 1998;
180 Turrigiano et al., 1998). At the NMJ in vivo, we could find no evidence for an increase in AChRs
181 after TTX block of the sciatic nerve in vivo (Wang et al., 2005). Is Rab3A required for the
182 homeostatic increase in surface AMPA-type glutamate receptors that has been confirmed by
183 multiple studies (see Introduction)?
184 In some studies of homeostatic synaptic plasticity it has been found that application of a
185 Ca^{2+}-permeable AMPA receptor-specific inhibitor reversed the homeostatic increase in mEPSC
186 amplitude (Ju et al., 2004; Thiagarajan et al., 2005; Sutton et al., 2006). Figure 3A shows that
187 the *TTX-induced increase* in mean mEPSC amplitude was nearly identical in a set of 11 CON and
188 11 TTX-treated cells before and after treatment with 1-Naphthyl acetyl spermine trihydrochloride
189 (NASPM), a synthetic analogue of the Ca^{2+}-permeable AMPA receptor inhibitor philanthotoxin
190 (before NASPM, CON 12.9 ± 3.5 pA; TTX, 17.5 ± 3.1 pA; after NASPM, CON 11.9 ± 2.6 pA; TTX
191 16.1 ± 3.5 pA). This result indicates that the TTX-induced increase in mEPSC amplitude does not
192 depend on Ca^{2+}-permeable receptors, since the effect of TTX clearly remained when their
193 presence was removed by acute NASPM application. We do not think that there was any
194 technical issue with the NASPM application, because overall, mEPSC amplitudes were reduced

195 modestly in both untreated and TTX-treated cultures (Figure 3B, CON, before NASPM, 12.9 ±
196 3.5 pA; after NASPM, 11.9 ± 2.6 pA; TTX, before NASPM, 17.5 ± 3.1 pA; after NASPM, 16.1 ± 3.5
197 pA). Furthermore, NASPM consistently reduced mEPSC frequency (Figure 3C, CON, before
198 NASPM, 1.84 $\pm$ 0.55 sec^{-1}; after NASPM, 1.56 $\pm$ 0.53 sec^{-1}; TTX, before NASPM, 4.40 ± 3.51 sec^{-1};
199 after NASPM, 2.68 ± 2.25 sec^{-1}). Similar to the data in Figure 1, frequency is significantly
200 increased after TTX treatment ($p = 0.04$), but this difference is no longer significant after
201 NASPM application ($p = 0.20$). One explanation for the effect on frequency is that there are
202 synaptic sites that express only homomers of Ca^{2+}-permeable AMPA receptors (GluA2-lacking
203 AMPARs); mEPSCs from these sites would be expected to be completely blocked by NASPM
204 (see cartoon description in Figure 3D, Left). We cannot rule out an alternative explanation, that
205 presynaptic Ca^{2+}-permeable AMPA receptors normally enhance release probability, and NAPSM
206 prevents this action. The magnitude of the frequency reduction following acute NASPM appears
207 to be greater after TTX treatment, suggesting that loss of activity could promote the
208 establishment of synaptic sites that contain only Ca^{2+}-permeable receptors. However, these
209 new sites do not appear to contribute to the increase in mEPSC amplitude (Figure 3A). The lack
210 of effect of NASPM rules out the contribution of homomeric Ca^{2+}-permeable AMPA receptors
211 GluA1, GluA3 and GluA4 (Hollmann et al., 1991; Burnashev et al., 1992; Jonas and Burnashev,
212 1995), as well as Ca^{2+}-permeable forms of Kainate receptors GluA5 and GluA6 (Koike et al.,
213 1997; Sun et al., 2009) to homeostatic synaptic plasticity.

214 Having established that homomeric Ca^{2+}-permeable receptors are not contributing to
215 the homeostatic increase in mEPSC amplitude, we turned to immunofluorescence and confocal
216 imaging to assess whether GluA2 receptor expression, which will identify GluA2 homomers and

217 GluA2 heteromers (the former unlikely to contribute to mEPSCs given their low conductance
218 relative to heteromers (Swanson et al., 1997; Mansour et al., 2001), was increased in our wild
219 type mouse cortical cultures following 48 hr treatment with TTX. Since mEPSCs necessarily
220 report synaptic levels of receptors, we used VGLUT1-immunofluorescence to identify synapses
221 on pyramidal primary apical dendrites labeled with MAP-2 immunofluorescence. We focused
222 on the primary dendrite of pyramidal neurons as a way to reduce variability that might arise
223 from being at widely ranging distances from the cell body, or, from inadvertently sampling
224 dendritic regions arising from inhibitory neurons. In addition, it has been shown that there is a
225 clear increase in response to glutamate in this region (Turrigiano et al., 1998). Figure 4 (Top)
226 shows two pyramidal neurons, one from an untreated culture on the left, and one from a TTX-
227 treated culture on the right, prepared from Rab3A$^{+/+}$ mice. To measure characteristics of
228 synaptically located GluA2 receptor clusters, we zoomed in on the primary dendrite (region in
229 white rectangle). The zoomed regions for single confocal sections of the selected area are
230 shown below and contain pairs of VGLUT1- and GluA2-immunofluorescent clusters indicated by
231 white trapezoidal frames. A dendrite typically required ~10 confocal sections to be fully
232 captured, and the total number of synaptic pairs for all the sections imaged on a dendrite
233 averaged 20 (20.4 $\pm$ 6.5 (SD); range, 11-38) so this is an atypically high number of pairs within a
234 single section; these particular dendrites and sections were selected for illustration purposes. In
235 addition to the synaptic pairs, we observed many GluA2-immunofluorescent clusters not
236 associated with VGLUT1 immunofluorescence (a few are indicated with white arrows), most
237 probably extrasynaptic receptors. There were also GluA2-positive clusters present outside of
238 MAP2-positive dendrites, which may be located on astrocytes (Fan et al., 1999). Finally, GluA2

239 immunofluorescent clusters close to VGLUT1 immunofluorescence but not located along any
240 apparent MAP2-positive neurites suggests the presence of axon-axonal contacts, although
241 VGLUT1 has also been detected in astrocytes (Ormel et al., 2012). Only sites that contained
242 both VGLUT1 and GluA2 immunofluorescence close to the primary MAP2-postive dendrite or a
243 secondary branch along this primary dendrite were selected for analyses. In the experiment
244 from which these images were collected, we analyzed the distance from the cell body for each
245 synapse. The average distance from the cell body, for dendrites from the untreated cell, was
246 38.5 $\pm$ 2.8 μm; for the TTX-treated cell, it was 42.4 $\pm$ 3.2 μm ($p = 0.35$, Kruskal-Wallis test). Since
247 the greatest distance from the cell body is set by the outer limit of the zoom window, and that
248 window was placed adjacent to the cell body, distances in other experiments would be in this
249 same range.

250 Variability in the magnitude of the homeostatic response from culture to culture is
251 averaged out in physiological experiments by the pooling of data from many cells across many
252 cultures. To reduce the necessity for many cultures, we chose to pair experiments in the same
253 cultures by recording mEPSCs from one set of coverslips, and processing another set of
254 coverslips from the same culture for immunofluorescence. We also wanted to determine if the
255 homeostatic response of mEPSC amplitudes varied from culture to culture, and if so, whether
256 the GluA2 receptor levels varied in parallel. We completed this matched paradigm of physiology
257 and immunofluorescence-for 3 cultures prepared from Rab3A$^{+/+}$ mice. We first present the
258 results as means for each culture, for control and TTX-treated dishes, for mEPSC data (Figure
259 5A) and imaging data (Figure 5B). Levels of GluA2 immunofluorescence at synaptic sites were
260 quantified by the size of the GluA2-immunofluorescent receptor cluster, because this showed

261 the greatest response to activity blockade; the average intensity value, and the integral of
262 intensity values across the area of the cluster, are included in a summary of the data in Table 1.
263 Three of three cortical cultures showed an increase in mean mEPSC amplitude after TTX
264 treatment. In contrast, one of the same three cultures showed a decrease in mean GluA2
265 receptor cluster size, suggesting that the decrease in receptor levels in Culture #3 was not due
266 to a lack of homeostatic effect on mEPSC amplitudes in that culture. Because there was a clear
267 trend towards increased GluA2 receptor cluster size, but the receptor response appears more
268 variable, we performed immunofluorescence measurements on two additional cortical
269 cultures, both of which showed modest increases after TTX treatment (Figure 5C). We
270 confirmed that there was also not a consistent increase in GluA1 receptor levels in two
271 matched cultures that showed robust homeostatic increases in mEPSC amplitudes
272 (Supplementary Figure 1A, culture mean mEPSC amplitudes; Supplementary Figure 1B, culture
273 mean GluA1 receptor cluster sizes).

274 We next pooled data from the multiple cultures to examine effects of activity blockade
275 on GluA2 receptors at the level of cell means. Because the average number of synaptic sites
276 identified in the primary dendrites in three cultures was 20.4, we also took 20 mEPSC samples
277 from each cell, the 21st to the 40th mEPSC recorded, to minimize any differences in variability
278 between GluA2 receptors and mEPSCs that might be due to a difference in sampling. In the
279 data pooled from the 3 matched experiments, neurons from Rab3A$^{+/+}$ cultures showed a
280 significant increase in mean mEPSC amplitudes following activity blockade (Figure 5D; Table 1).
281 This result indicates that the homeostatic response averaged across the 3 cultures was very
282 similar to, but slightly smaller than, that of the data set presented in Figure 1. The mean for size

283 of GluA2 immunofluorescent receptor clusters showed a trend towards higher values after
284 activity blockade (18.1%) that was of similar magnitude to the mEPSC amplitude increase
285 (19.7%), but did not reach statistical significance for 3 cultures (Figure 5E) or 5 cultures (Figure
286 5F; Table 1). As expected, mean mEPSC amplitude was not increased following activity
287 blockade in the data pooled from a new set of 3 Rab3A$^{-/-}$ cultures (Table 1). For
288 immunofluorescence results from the same Rab3A$^{-/-}$ cultures, no trend towards higher values
289 was apparent for GluA2 receptor cluster characteristics (Table 1). However, given the variability
290 of the GluA2 response in cultures from Rab3A$^{+/+}$ mice, it would require a much higher number
291 of Rab3A$^{+/+}$ and Rab3A$^{-/-}$ cultures to make any firm conclusions about the role of Rab3A in the
292 homeostatic response of GluA2 receptors.

293 Having used VGLUT1 immunofluorescence to mark synaptic sites, we could also ask
294 whether there was a presynaptic effect of activity blockade on the size, intensity or integral of
295 the VGLUT1 signal at sites apposed to the previously examined GluA2 postsynaptic sites. In the
296 pooled data from cultures prepared from Rab3A$^{+/+}$ mice, we found no change in the size of the
297 VGLUT1-positive regions, and trends towards reduced intensity and integral (Table 2). These
298 data do not support the idea that activity blockade caused an increase in the amount of
299 VGLUT1 per vesicle, although we cannot rule out that a simultaneous reduction in the number
300 of vesicles obscured the effect, since we did not have an independent label for synaptic
301 vesicles. In cultures prepared from Rab3A$^{-/-}$ mice, the size, intensity and integral of the VGLUT1-
302 positive regions did not significantly change (Table 2).

303 We have demonstrated here for the first time that the synaptic vesicle protein Rab3A
304 influences the homeostatic regulation of quantal amplitude. What are possible ways that

305 Rab3A could exert its effect? It has previously been shown that exogenous addition of TNFα to
306 hippocampal cultures causes an increase in surface expression of GluA1 receptors (although not
307 GluA2 receptors), and that the homeostatic increase in mEPSC amplitudes is abolished in
308 cultures prepared from the TNFα deletion mouse (Stellwagen et al., 2005; Stellwagen and
309 Malenka, 2006). Furthermore, neurons from TNF$\alpha^{+/+}$ mice plated on glial feeder layers derived
310 from TNF$\alpha^{-/-}$ mice fail to show the increase in mEPSC amplitude after TTX treatment, indicating
311 that the TNFα inducing the receptor increases following activity blockade comes from the glial
312 cells (Stellwagen and Malenka, 2006). It has recently been shown that the source of TNFα is
313 astrocytes rather than microglia (Heir et al., 2024).

314 Rab3A has been detected in astrocytes (Maienschein et al., 1999; Hong et al., 2016), so
315 to determine whether Rab3A is acting via regulating TNFα release from astrocytes, we
316 performed experiments similar to those of Stellwagen and Malenka (2006) (schema illustrated
317 in Figure 6, Left). Under our culturing conditions, the glial feeder layers would be expected to
318 be composed mainly of astrocytes (Heir et al., 2024). We compared the effect of activity
319 blockade on mEPSC amplitudes recorded from cortical neurons from Rab3A$^{+/+}$ mice plated on
320 Rab3A$^{+/+}$ glial feeder layers (Figure 6A); neurons from Rab3A$^{+/+}$ mice plated on Rab3A$^{-/-}$ glia
321 (Figure 6B), and neurons from Rab3A$^{-/-}$ mice plated on Rab3A$^{+/+}$ glia (Figure 6C). If Rab3A is
322 required for TNFα release from glia, then Rab3A$^{+/+}$ neurons plated on Rab3A$^{-/-}$ glia should not
323 show a homeostatic increase in mEPSC amplitude after treatment with TTX, and any cultures
324 with Rab3A$^{+/+}$ glia should have a normal homeostatic response. We found the opposite result:
325 mEPSC amplitudes increased in cultures where Rab3A was present in neurons (WT on WT, CON,
326 13.3 $\pm$ 0.5 pA, TTX, 16.7 $\pm$ 1.2 pA; WT on KO, CON, 13.3 $\pm$ 1.0 pA, TTX, 18.8 $\pm$ 1.4 pA), but the

327 increase was greatly diminished in cultures where Rab3A was present only in glia (KO on WT,
328 CON, 15.2 $\pm$ 1.1 pA, TTX, 16.9 $\pm$ 0.7 pA). In the glial feeder layer culture, the loss of Rab3A in the
329 neurons may have caused an increase in mEPSC amplitude at baseline, similar to the Earlybird
330 mutant in dissociated cultures, but this difference was not significant (CON, WT on WT, 13.3
331 $\pm$ 0.5 pA; CON, KO on WT, 15.2 $\pm$ 1.1 pA, p = 0.78, Tukey's post-hoc test after two-way ANOVA).
332 Regarding mEPSC frequency, in cultures with Rab3A$^{+/+}$ neurons, frequency trended upward
333 after activity blockade, whereas in the culture with Rab3A$^{-/-}$ neurons, frequency was already
334 increased (although not significantly, CON, WT on WT, 2.54 $\pm$ 0.57 sec^{-1}; CON, KO on WT, 4.46 $\pm$
335 1.21 sec^{-1}, p = 0.59, Tukey's), and trended downward after activity blockade.
336 In summary, in the absence of Rab3A from glia, the homeostatic plasticity of mEPSC
337 amplitude following activity blockade was normal, whereas in the absence of Rab3A in neurons,
338 homeostatic plasticity was greatly diminished. This result makes it highly unlikely that Rab3A is
339 required for the release of TNFα, or another factor from glia, that induces a homeostatic
340 upregulation of postsynaptic receptors and thereby increases mEPSC amplitude following TTX
341 treatment. Neuronal Rab3A appears to mediate the homeostatic increase in mEPSC amplitude
342 following activity blockade.

343

344 Discussion

345 We found that homeostatic synaptic plasticity of mEPSC amplitude in dissociated mixed
346 cultures of mouse cortical neurons and glia behaved remarkably similar to the mouse NMJ in
347 response to loss of Rab3A function: in cultures from Rab3A$^{-/-}$ mice, the increase in mEPSC

348 amplitudes following prolonged network silencing by TTX was strongly diminished, and in
349 cultures from Rab3A$^{Ebd/Ebd}$ mice, basal mEPSC amplitude was increased compared to that of
350 wild-type cultures and was not further modified by TTX treatment. These results suggest that
351 normal function of the synaptic vesicle protein Rab3A is required for the homeostatic increase
352 of mEPSC amplitude in cortical cultures.

353

354 *Is Rab3A acting in the presynaptic cell to cause homeostatic increase in mEPSC amplitude?*

355 The impetus for our current study was two previous studies in which we examined
356 homeostatic regulation of quantal amplitude at the NMJ. An advantage of studying the NMJ is
357 that synaptic ACh receptors are easily identified with fluorescently labeled α-bungarotoxin,
358 which allows for very accurate quantification of postsynaptic receptor density. We were able to
359 detect a known change due to mixing 2 colors of α-bungarotoxin to within 1% (Wang et al.,
360 2005). Using this model synapse, we showed that there was no increase in synaptic AChRs after
361 TTX treatment, whereas miniature endplate current increased 35% (Wang et al., 2005). We
362 further showed that the presynaptic protein Rab3A was necessary for full upregulation of mEPC
363 amplitude (Wang et al., 2011). These data strongly suggested Rab3A contributed to
364 homeostatic upregulation of quantal amplitude via a presynaptic mechanism. With the current
365 study showing that Rab3A is required for the homeostatic increase in mEPSC amplitude in
366 cortical neuron cultures, one interpretation is that in both situations, Rab3A is required for an
367 increase in the presynaptic quantum.

368 The presynaptic quantum, or the amount of transmitter released during a single fusion
369 event, is an important contributor to quantal size. The amount of transmitter released during
370 vesicle fusion can be affected by the kinetics of the fusion pore opening (Chang et al., 2017).
371 We previously used amperometric measurements in mouse adrenal chromaffin cells to show
372 loss of Rab3A increased the occurrence of very small amplitude fusion pore feet (Wang et al.,
373 2008). Paired with our finding that there is an increase in the occurrence of very slow-rising,
374 abnormally shaped mEPCs at the neuromuscular junction of Rab3A$^{-/-}$ mice, our data suggest
375 that small synaptic vesicles may have a fusion pore step under certain circumstances (see also
376 (Chiang et al., 2018)). If activity blockade causes an increase in mEPSC amplitude due to a more
377 rapid opening of a fusion pore, or a larger fusion pore conductance, it is possible that Rab3A is
378 required for this modulation.

379 Another way to increase the presynaptic quantum is to increase levels of the transmitter
380 transporter (Daniels et al., 2004; De Gois et al., 2005; Wilson et al., 2005; Hartman et al., 2006).
381 However, we found that immunofluorescence for the glutamate transporter, VGLUT1, was not
382 increased after activity blockade under our experimental conditions. A similar lack of increase in
383 VGLUT1 levels, relative to synapsin, was previously observed in hippocampal cultures treated
384 with NBQX, an AMPA receptor blocker (see supplemental data, (Wilson et al., 2005)). Taken
385 together with our findings, it appears that there is not strong evidence that the amount of
386 VGLUT1 at synapses is a contributing factor to the increase in mEPSC amplitude in neuronal
387 cultures after activity blockade with TTX.

388 Finally, the amount of transmitter released by a vesicle could be increased due to larger
389 vesicle size. Larger vesicle diameter has been observed following activity disruption in multiple

390 paradigms, including ocular deprivation, cortical ablation, and immobilization (Kawana et al.,
391 1971; Lloret and Saavedra, 1975; Cheresharov et al., 1978). Loss of Rab3 family members is
392 associated with increased vesicle size (Riedel et al., 2002; Schonn et al., 2010). An increase in
393 volume has been shown to increase miniature endplate junctional current amplitude at the
394 Drosophila NMJ (Karunanithi et al., 2002). Rab3A could be required for an activity-dependent
395 increase in vesicle size, but the increase in diameter needed for a 25% increase in transmitter,
396 and therefore mEPSC amplitude (~3%), would be difficult to detect.

397

398 *Is Rab3A acting on postsynaptic receptors to cause increase in mEPSC amplitude?*

399 In neurons, the increase in mEPSC amplitude following block of activity was not due to
400 increases in Ca^{2+}-permeable GluA1 homomers because acute NASPM application was unable to
401 reverse the TTX-induced increase in amplitude. While we found that the effect of TTX
402 treatment on mEPSC amplitude and GluA2 receptor levels were of similar magnitude, the effect
403 on GluA2 receptor levels was not statistically significant for the pooled data sets acquired in the
404 same 3 cultures, nor in a larger data set containing an additional 2 cultures. In light of the
405 extensive literature documenting increases in GluA1 or GluA2 receptors, or both, after activity
406 blockade, the less than convincing increase in GluA2 receptor levels in the current work came
407 as a surprise. The reason for the lack of significance was that the increase in receptors was
408 more variable. We are aware of three possible explanations for greater variability. 1) The
409 number of synaptic sites sampled was smaller for the imaging data set. This was because we
410 limited our analysis to synaptic receptors on the primary dendrite, where a clear increase in

411 sensitivity to exogenously applied glutamate was demonstrated (see Figure 3 in (Turrigiano et
412 al., 1998)). To address this issue, we limited our sample size of mEPSCs in the matched
413 experiments to the same number per cell as the mean sample size per cell for imaging, but
414 there was still a discrepancy in the effect of TTX on mEPSCs vs. receptors. 2) The small sample
415 of only 3 cultures was not enough to reveal the increase in receptors. We attempted to address
416 this by adding 2 more cultures. Although both additional cultures showed small increases in
417 GluA2 receptor cluster size, when cells from these cultures were included in the pooled data
418 set, the p value was not substantially improved. A remaining possibility is: 3) The complexity
419 involved in processing cultures for immunofluorescence introduces variability that obscures the
420 true effect. One can get around technical issues related to immunofluorescence processing by
421 performing Western blots, but then any changes detected could be due to upregulation of
422 extrasynaptic receptors.

423 What remains unclear is why our data were impacted by the variability inherent in
424 immunofluorescence measurements, but data of other studies were not. Some other studies
425 have used the number of synaptic sites or puncta as the sample size (for example, (Hou et al.,
426 2008; Ibata et al., 2008; Wang et al., 2019)). When we analyzed our data after including as few
427 as 6 randomly selected cluster size measurements per cell, a Kruskal-Wallis test gave highly
428 significant p values for 3 cultures ($p = 0.001$, $n = 174$ sites (6 *29 cells)) and 5 cultures ($p =$
429 0.005, $n = 294$ sites (6 *49 cells)). We found only a single study that had comparable sample
430 sizes for receptors and mEPSC amplitudes, and the p value was < 0.01 for mEPSC amplitudes (n
431 $= 9$ and 10 cells for CON and TTX, respectively), but five times higher (< 0.05) for receptor data
432 ($n = 13$ and 14 cells for CON and TTX) (Xu and Pozzo-Miller, 2017). This single example is

433 consistent with our suggestion that measurements of changes in receptors after activity
434 blockade are more variable than measurements of mEPSC amplitudes. In sum, the lack of a
435 robust increase in receptor levels leaves open the possibility that there is a presynaptic
436 contributor to quantal size in mouse cortical cultures. However, the variability could arise from
437 technical factors associated with the immunofluorescence method, and the mechanism of
438 Rab3A-dependent homeostatic plasticity could be presynaptic for the NMJ and postsynaptic for
439 cortical neurons.

440 Increased receptors likely contribute to increases in mEPSC amplitudes, but because we
441 do not have a significant increase in GluA2 receptors in our experiments, it is impossible to
442 conclude that the increase is lacking in cultures from Rab3A$^{-/-}$ neurons. Furthermore, without
443 additional experiments targeting Rab3A deletion to the pre- or post-synaptic compartment, we
444 cannot rule out that Rab3A is regulating homeostatic plasticity in mouse cortical cultures by
445 acting postsynaptically on receptor trafficking. To our knowledge, there is no evidence localizing
446 Rab3A to postsynaptic dendritic sites, although other presynaptic molecules, such as SNARE
447 proteins, synaptotagmins, and NSF, have been identified in the postsynaptic compartment
448 (Lledo et al., 1998; Nishimune et al., 1998; Osten et al., 1998; Song et al., 1998; Araki et al.,
449 2010; Kennedy et al., 2010; Suh et al., 2010; Jurado et al., 2013; Hussain and Davanger, 2015;
450 Gu et al., 2016; Wu et al., 2017). A recent report implicates Rab3A in the localization of plasma
451 membrane proteins, including the EGF receptor, in rafts in HEK cells and Jurkat-T cells, which
452 indicates Rab3A can be found in other specialized locations besides the presynaptic nerve
453 terminal (Diaz-Rohrer et al., 2023).
454

455 *Neuronal, not glial, Rab3A is required for homeostatic regulation of quantal amplitude*

456 Astrocytic release of TNFα was shown to mediate the increase in mEPSC amplitudes in
457 prolonged TTX-treated cultures of dissociated hippocampal neurons and cultures of
458 hippocampal slices (Stellwagen and Malenka, 2006; Heir et al., 2024). TNF-α accumulates after
459 activity blockade, and directly applied to neuronal cultures, can cause an increase in GluA1
460 receptors, providing a potential mechanism by which activity blockade leads to the homeostatic
461 upregulation of postsynaptic receptors (Beattie et al., 2002; Stellwagen et al., 2005; Stellwagen
462 and Malenka, 2006). However, we found that loss of Rab3A in glia did not disrupt the increase
463 in mEPSC amplitude after activity blockade, so it is unlikely that the Rab3A-dependent
464 homeostatic increase in mEPSC amplitude is via the astrocytic-TNF-α pathway. Interestingly, we
465 previously showed that the homeostatic increase in NMJ mEPC amplitude was completely
466 normal in the absence of TNF-α (Wang et al., 2011), suggesting the possibility that neuronal
467 Rab3A can act via a non-TNF-α mechanism to contribute to homeostatic regulation of quantal
468 amplitude, although we have not ruled out a neuronal Rab3A-mediated TNF-α pathway in
469 cortical cultures.

470

471 *Is the lack of homeostatic plasticity in the Earlybird mutant due to occlusion?*

472 We found that mEPSC amplitude was increased in untreated cultures prepared from
473 Rab3A$^{Ebd/Ebd}$ mice, compared to mEPSC amplitude in cultures from wild type mice. If there is a
474 limit to how large an mEPSC can become, it is possible that the mutant Rab3A does not affect
475 homeostatic plasticity, only occludes it. Similar increases in mEPSC amplitude at baseline,

476 combined with a failure to increase further after activity blockade, were noted in cultures
477 prepared from mECP2, AKAP, Homer1a, and Arc/Arg3.1 deletion mice (Shepherd et al., 2006;
478 Hu et al., 2010; Xu and Pozzo-Miller, 2017; Sanderson et al., 2018) as well as in cultures treated
479 with ubiquitin proteasome inhibitors (Jakawich et al., 2010) or microRNA 186-5p (Silva et al.,
480 2019), suggesting the possibility of a generalized phenomenon in which increased mEPSC
481 amplitude is induced when homeostatic regulation is disrupted. Since we did not observe such
482 an increase in mEPSC amplitude at baseline in cultures from Rab3A$^{-/-}$ mice, it remains a
483 possibility that the point mutant may bind to novel partners, causing activities that would not
484 be either facilitated or inhibited by Rab3A. Still, it is a strong coincidence that the novel activity
485 of the mutant Earlybird Rab3A would affect mEPSC amplitude, the same characteristic that is
486 modulated by activity blockade in a Rab3A dependent manner. Although we cannot rule out
487 occlusion, an alternate interpretation is that the presence of the mutant protein mimics the
488 condition of activity blockade.

489

490 *Rab3A is the first presynaptic function protein required for full homeostatic plasticity of mEPSC*
491 *amplitude*

492 The number of molecules shown to be required for homeostatic synaptic plasticity of
493 quantal size in neuronal cultures may have surpassed ~20 (see (Koesters et al., 2024) for a
494 recent summary), but fall into two main categories: molecules involved in glutamate receptor
495 expression or trafficking, and signaling molecules. To our knowledge, this is the first evidence
496 that a presynaptic protein is participating in this process. Homeostatic synaptic plasticity is
497 becoming increasingly implicated in essential normal functions such as sleep (Tononi and Cirelli,

498 2014; Diering et al., 2017; Torrado Pacheco et al., 2021), and pathological conditions such as
499 epilepsy, neuropsychiatric disorders, Huntington's, and alcohol use disorder (Trasande and
500 Ramirez, 2007; Fernandes and Carvalho, 2016; Wang et al., 2017; Lovinger and Abrahao, 2018;
501 Smith-Dijak et al., 2019; Lignani et al., 2020; Suzuki et al., 2021; Kavalali and Monteggia, 2023).
502 Therefore, our identification of a novel Rab3A-dependent regulatory pathway in homeostatic
503 synaptic plasticity may have important therapeutic implications. Our findings also further
504 cement the importance of Rab3A in activity-dependent modulation of synaptic strength.

505

506 Materials and Methods

507 *Animals.* To determine the role of Rab3A in homeostatic plasticity in mouse cortical cultures,
508 we employed two distinct genetic mouse strains with altered Rab3A function. Rab3A deletion
509 mice were generated as follows: Rab3A$^{+/-}$ heterozygous mice were bred and genotyped as
510 previously described (Kapfhamer et al., 2002; Wang et al., 2008), and maintained as a colony
511 using multiple heterozygous breeding pairs. Homozygous Rab3A$^{+/+}$ or Rab3A$^{-/-}$ mouse pups
512 were obtained by breeding Rab3A$^{+/+}$ pairs and Rab3A$^{-/-}$ pairs, respectively, so that the pups
513 were the first-generation progeny of a homozygous mating. This protocol minimizes the
514 tendency of multiple generations of Rab3A$^{+/+}$ and Rab3A$^{-/-}$ homozygous breedings to produce
515 progeny that are more and more genetically distinct. Rab3A$^{Ebd/Ebd}$ mice were identified in an
516 EU-mutagenesis screen of C57BL/6J mice, and after a cross to C3H/HeJ, were backcrossed for 3
517 generations to C57BL/6J (Kapfhamer et al., 2002). Rab3A$^{+/Ebd}$ heterozygous mice were bred at
518 Wright State University and genotyped in a two-step procedure: 1. a PCR reaction (forward
519 primer: TGA CTC CTT CAC TCC AGC CT; reverse primer: TGC ACT GCA TTA AAT GAC TCC T)

520 followed by 2. a restriction digest with enzyme Bsp1286I (New England Biolabs) that
521 distinguishes the Earlybird mutant by its different base-pair products. Rab3A$^{+/-}$ mice were
522 backcrossed with Rab3A$^{+/+}$ mice from the Earlybird heterozygous colony for 11 generations in
523 an attempt to establish a single wild type strain, but differences in mEPSC amplitude and
524 adrenal chromaffin cell calcium currents persisted, likely due to genes that are close to the
525 Rab3A site, resulting in two wild type strains: 1. Rab3A$^{+/+}$ from the Rab3A$^{+/-}$ colony, and 2.
526 Rab3A$^{+/+}$ from the Rab3A$^{+/Ebd}$ colony.

527 *Primary Culture of Mouse Cortical Neurons.* Primary dissociated cultures of mixed neuronal and
528 glia populations were prepared as previously described (Hanes et al., 2020). Briefly, postnatal
529 day 0-2 (P0-P2) Rab3A$^{+/+}$, Rab3A$^{-/-}$ or Rab3A$^{Ebd/Ebd}$ neonates were euthanized by rapid
530 decapitation, as approved by the Wright State University Institutional Animal Care and Use
531 Committee, and brains were quickly removed. Each culture was prepared from the cortices
532 harvested from two animals; neonates were not sexed. Cortices were collected in chilled
533 Neurobasal-A media (Gibco) with osmolarity adjusted to 270 mOsm and supplemented with 40
534 U/ml DNAse I (ThermoFisher Scientific). The tissues were digested with papain (Worthington
535 Biochemical) at 20 U/ml at 37°C for 20 minutes followed by trituration with a sterile, fire-
536 polished Pasteur pipette, then filtered through a 100 μm cell strainer, and centrifuged at 1100
537 rpm for 2 minutes. After discarding the supernatant, the pellet was resuspended in room
538 temperature Neurobasal-A media (270 mOsm), supplemented with 5% fetal bovine serum for
539 glia growth, and 2% B-27 supplement to promote neuronal growth (Gibco), L-glutamine, and
540 gentamicin (ThermoFisher Scientific). Neurons were counted and plated at $0.15 * 10^6$
541 cells/coverslip onto 12 mm coverslips pre-coated with poly-L-lysine (BioCoat, Corning). This

542 plating density produces a “high density” culture characterized by a complex mesh of neuronal
543 processes criss-crossing the field of view, completely filling the space between cell bodies (see
544 Figure 4). We found in preliminary experiments that an increase in mEPSC amplitude in mouse
545 cortical cultures was inconsistent when cell density was low, likely due to lower levels of
546 baseline activity, although it is a limitation of this study that we did not directly measure activity
547 levels in cultures prepared from Rab3A$^{+/+}$, Rab3A$^{-/-}$ or Rab3A$^{Ebd/Ebd}$ mice, and therefore do not
548 know if differences in results are due to differences in activity levels. While unlikely for Rab3A$^{+/+}$
549 and Rab3A$^{-/-}$ studies, given the mEPSC amplitude in untreated cultures was relatively small, it
550 remains possible that in Rab3A$^{Ebd/Ebd}$ studies, the larger mEPSC amplitude in untreated cultures
551 was due to a loss of activity in these cultures. The culture media for the first day (0 DIV) was the
552 same as the above Neurobasal-A media supplemented with FBS, B-27, L-glutamine, and
553 gentamicin, and was switched after 24 hours (1 DIV) to media consisting of Neurobasal-A (270
554 mOsm), 2% B-27, and L-glutamine without FBS to avoid its toxic effects on neuronal viability
555 and health (Stellwagen and Malenka, 2006). Half of the media was changed twice weekly and
556 experiments were performed at 13-14 DIV. Two days prior to experiments, tetrodotoxin (TTX)
557 (500 nM; Tocris), a potent Na^+ channel blocker, was added to some cultures to chronically
558 silence all network activity and induce homeostatic synaptic plasticity mechanisms, while
559 untreated sister cultures served as controls. Cultures prepared from mutant mice were
560 compared with cultures from wild-type mice from their respective colonies. Note that the
561 cultures comprising the Rab3A$^{+/+}$ data here are a subset of the data previously published in
562 Hanes et al., 2020. This smaller data set was restricted to the time period over which cultures
563 were also prepared from Rab3A$^{-/-}$ mice.

564 *Preparation of Glial Feeder Layers.* Glial feeder layers were prepared from the cortices of P0-P2
565 Rab3A$^{+/+}$ or Rab3A$^{-/-}$ mouse pups as described previously (Stellwagen and Malenka, 2006).
566 Briefly, cortices were dissected and cells were dissociated as described above. Cell suspensions
567 of mixed neuronal and glial populations were plated onto glass coverslips pre-coated with poly-
568 L-lysine in Dulbecco's Modified Eagle Media (ThermoFisher Scientific) supplemented with 5%
569 FBS (to promote glial proliferation and to kill neurons), L-glutamine, and gentamicin, and
570 maintained in an incubator at 37°C, 5% CO_2; cultures were maintained in this manner for up to
571 1 month to generate purely glial cultures (all neurons typically died off by 7 DIV). Culture media
572 was replaced after 24 hours, and subsequent media changes were made twice weekly,
573 replacing half of the culture media with fresh media. Feeder layers were not used for neuronal
574 seeding until all native neurons were gone and glia approached 100% confluency (visually
575 inspected).
576 *Plating of Neurons on Glial Feeder Layers.* Cortical neurons were obtained as described above.
577 The cell pellet obtained was resuspended in Neurobasal-A (osmolarity adjusted to 270 mOsm)
578 containing B27 (2%, to promote neuronal growth), L-glutamine, and 5-fluorodeoxyuridine (FdU,
579 a mitotic inhibitor; Sigma). Addition of FdU was used to prevent glial proliferation and
580 contamination of the feeder layer with new glia, promoting only neuronal growth on the feeder
581 layers (FdU-containing media was used for the maintenance of these cultures and all
582 subsequent media changes). Glial culture media was removed from the feeder layer cultures,
583 and the neuronal cell suspension was plated onto the glial feeder cultures. The culture strategy
584 used to distinguish the relative roles of neuronal and glial Rab3A is outlined in Figure 8, Left. At
585 1 DIV, all of the culture media was removed and replaced with fresh Neurobasal-A media

586 containing FdU described above, and half of the media was replaced twice per week for all
587 subsequent media changes. Cultures were maintained in a 37°C, 5% CO_2 incubator for 13-14
588 DIV.
589 *Whole-Cell Voltage Clamp to Record mEPSCs*. At 13-14 DIV, mEPSCs from TTX-treated and
590 untreated sister cultures of Rab3A$^{+/+}$ or Rab3A$^{-/-}$ neurons from the Rab3A$^{+/-}$ colony, or Rab3A$^{+/+}$
591 or Rab3A$^{Ebd/Ebd}$ neurons from the Rab3A$^{+/Ebd}$ colony, were recorded via whole-cell voltage clamp
592 to assess the role of Rab3A in homeostatic synaptic plasticity. Recordings were taken from
593 pyramidal neurons, which were identified visually by a prominent apical dendrite; images were
594 taken of all cells recorded from. Cells were continuously perfused with a solution consisting of
595 (in mM): NaCl (115), KCl (5), $CaCl_2$ (2.5), $MgCl_2$ (1.3), dextrose (23), sucrose (26), HEPES (4.2),
596 pH = 7.2 (Stellwagen and Malenka, 2006). On the day of recording, the osmolarity of the media
597 from the cultures was measured (normally 285 – 295 mOsm) and the perfusate osmolarity was
598 adjusted to match the culture osmolarity to protect against osmotic shock to the neurons. To
599 isolate glutamatergic mEPSCs, TTX (500 nM) and picrotoxin (50 µM), were included in the
600 perfusion solution to block action potentials and GABAergic currents, respectively. The NMDA
601 receptor antagonist, APV, was not included in the perfusion solution because in pilot studies, all
602 mEPSCs were blocked by 10 µM CNQX and 50 µm picrotoxin, demonstrating no APV-sensitive
603 mEPSCs were present (data not shown). Previous studies have described NMDA mEPSCs in
604 neuronal cultures, but recordings were performed in 0 Mg^{2+} (Watt et al., 2000; Sutton et al.,
605 2006). In our recordings, the presence of extracellular Mg^{2+} (1.3 mM) <u>and</u> TTX would mean that
606 the majority of NMDA receptors are blocked by extracellular Mg^{2+} at resting Vm. Patch
607 electrodes (3.5 – 5 MΩ) were filled with an internal solution containing (in mM): K-gluconate

608 (130), NaCl (10), EGTA (1), $CaCl_2$ (0.132), $MgCl_2$ (2), HEPES (10), pH = 7.2. Osmolarity was
609 adjusted to 10 mOsm less than the perfusion solution osmolarity, which we have found
610 improves success rate of achieving low access resistance recordings. Neurons were clamped at
611 a voltage of -60 mV using an Axopatch 200B patch-clamp (Axon Instruments), recorded from for
612 2 – 5 minutes, and data were collected with Clampex 10.0/10.2 (Axon Instruments).
613 *NASPM application*. The antagonist of Ca^{2+}-permeable AMPA receptors, N-naphthyl
614 acetylspermine (NASPM, 20 μM; Tocris), was applied during recordings in a subset of
615 experiments. NASPM is a synthetic analog of Joro Spider Toxin (JSTX) (Koike et al., 1997), and
616 chemicals in this family block Ca^{2+} permeable glutamate receptors (Blaschke et al., 1993;
617 Herlitze et al., 1993; Iino et al., 1996). The presence of the edited GluA2 subunit disrupts both
618 the Ca^{2+} permeability and the sensitivity to JSTX and related substances (Blaschke et al., 1993;
619 Bochet et al., 1994; Jonas and Burnashev, 1995). Therefore, 20 μM NASPM is expected to
620 completely block AMPA receptors containing GluA1, GluA3 or GluA4 subunits (Hollmann et al.,
621 1991; Burnashev et al., 1992), or the Kainate receptors containing GluA5 or GluA6 (Koike et al.,
622 1997; Sun et al., 2009), but be ineffective against any heteromer or homomer containing GluA2
623 subunits. Because the effect of the spider toxins and their analogues are use-dependent
624 (Herlitze et al., 1993; Iino et al., 1996; Koike et al., 1997), NASPM was applied with a
625 depolarizing high K^+ solution (25 mM KCl, 95 mM NaCl) which we expected to trigger release of
626 glutamate and opening of glutamate-activated receptors, allowing entry of NASPM into the
627 pore. Baseline recordings were performed for 2 minutes in our standard perfusate, followed by
628 perfusion of NASPM + High K^+ solution for 45 seconds, and then perfusion of a NASPM only

629 solution for 5 minutes, after which recording was recommenced for 5 minutes (because we
630 found in pilot experiments that frequency was reduced following NASPM application).
631 *Analysis of mEPSCs.* Miniature excitatory postsynaptic currents (mEPSCs) were manually
632 selected using Mini Analysis software (Synaptosoft), a standard program used for mEPSC event
633 detection and analysis. Records were filtered at 2 kHz using a low-pass Butterworth filter prior
634 to selection. The program detection threshold was set at 3 pA but the smallest mEPSC selected
635 was 4.01 pA. A fully manual detection process means that the same criterion ("does this *look*
636 like an mEPSC?") is applied to all events, not just the false positives or the false negatives,
637 which prevents the bias from being primarily at one end or the other of the range of mEPSC
638 amplitudes. It is important to note that when performing the MiniAnalysis process, the
639 researcher did not know whether a record was from an untreated cell or a TTX-treated cell.
640 *Immunofluorescence, microscopy, and data analysis.* Primary cultures of mouse cortical
641 neurons were grown for 13-14 DIV. Antibodies to GluA2 (mouse ab against N-terminal, EMD
642 Millipore) were added directly to live cultures at 1:40 dilution, and incubated at 37 °C in a CO_2
643 incubator for 45 minutes. Cultures were rinsed 3 times with PBS/5% donkey serum before being
644 fixed with 4% paraformaldehyde. After 3 rinses in PBS/5% donkey serum, cultures were
645 incubated in CY3-labeled donkey-anti-mouse secondary antibodies for 1 hour at room
646 temperature, rinsed in PBS/5% donkey serum, permeabilized with 0.2% saponin, and incubated
647 in chick anti-MAP2 (1:2500, AbCAM) and rabbit anti-VGLUT1 (1:4000, Synaptic Systems) for 1
648 hour at room temperature in PBS/5% donkey serum. After rinsing with PBS/5% donkey serum,
649 coverslips were incubated with 488-anti chick and CY5-anti rabbit secondary antibodies for 1
650 hour at room temperature, rinsed, blotted to remove excess liquid, and inverted on a drop of

651 Vectashield (Vector Labs). Coverslips were sealed with nail polish and stored at 4 °C for < 1
652 week before imaging. All secondary antibodies were from Jackson Immunoresearch and were
653 used at 1:225 dilution.

654 Coverslips were viewed on a Fluoview FV1000 laser scanning confocal microscope with a
655 60x oil immersion, 1.35 NA objective. Once a pyramidal neuron was identified and a single
656 confocal section of the cell acquired (see Top, Figure 4), Fluoview 2.1 software was used to
657 zoom in on the primary dendrite (5X) and a series of confocal sections were taken every 0.5
658 μm. Images were analyzed offline with ImagePro 6 (Cybernetics). The composite image was
659 used to locate synaptic sites containing both VGLUT1 and GluA2 immunoreactivity in close
660 apposition to each other and to the primary dendrite or a secondary branch identified with
661 MAP2 immunoreactivity. An area of interest (AOI) was manually drawn around the GluA2
662 cluster in the confocal section in which it was the brightest. The AOIs for a dendrite were saved
663 in a single file; the AOI number and the confocal section it was associated with were noted for
664 later retrieval. For quantification, AOIs were loaded, an individual AOI was called up on the
665 appropriate section, and the count/measurement tool used to apply a threshold. Multiple
666 thresholds were used, 400-550, but we found that within a given experiment, the magnitude of
667 the TTX effect was not altered by different thresholds, therefore, all data presented here use a
668 threshold of 450. Pixels within the cluster that were above the threshold were automatically
669 outlined, and size, average intensity, and integral of the outlined region saved to Origin2020
670 (OriginLab) file for calculating mean values. For analyzing VGLUT1 sites, previous AOIs were
671 examined, and if not directly over the VGLUT1 site, moved to encompass it (this happened
672 when GluA2 and VGLUT1 were side by side rather than overlapping). The threshold was 200 for

673 all VGLUT1 data except Rab3A$^{+/+}$ Culture #1, where threshold was 400. There was no threshold
674 that worked for both that culture and the other cultures, with too much of the background
675 regions being included for Culture #1 with a threshold of 200, and too little of the synaptic site
676 area being included for the other Cultures with a threshold of 400.

677 *Statistics.* In our previous publication (Hanes et al., 2020), we described the characteristics of
678 homeostatic plasticity of mEPSC amplitudes in mouse cortical cultures using multiple mEPSC
679 amplitude quantiles from each cell to create data sets with thousands of samples. We
680 compared the cumulative distribution functions for mEPSC amplitudes in untreated vs. TTX-
681 treated cultures, as well as sorting the values from smallest to largest, and plotted TTX values
682 vs. control values in the rank order plot first described in (Turrigiano et al., 1998) to
683 demonstrate synaptic scaling. Finally, we plotted the ratio of TTX values/control values vs.
684 control values to show that the ratio, which represents the effect of TTX, increased with
685 increasing control values, which we termed "divergent scaling." Here, we wanted to avoid the
686 inflation of sample size caused by pooling multiple mEPSCs per cell. To statistically compare the
687 effects of TTX in cultures of wild type mice, Rab3A$^{-/-}$ mice and Rab3A$^{Ebd/Ebd}$ mutant mice, or, WT-
688 WT, WT-KO and KO-WT neuron-glial cultures, we performed a two-way ANOVA, followed by a
689 Tukey test, and used the p value for each specific situation (for example, CON vs. TTX for
690 Rab3A$^{+/+}$; CON vs. TTX for Rab3A$^{-/-}$, and so on. The overall means are presented ± SEM in the
691 text, and p values are displayed above each plot, with N = the number of cells. For the
692 characteristics of synaptic GluA2 receptor clusters and VGLUT1 sites in imaging experiments,
693 with N = the number of dendrites (one dendrite was sampled for each cell), and statistical
694 comparisons were made with the non-parametric Kruskal-Wallis test. Although we quantified

695 three characteristics of the GluA2 clusters and VGLUT1 sites, size, average intensity, and
696 integral, we have not corrected p values for multiple comparisons. Means are presented as box
697 plots + data, with the box at 25 and 75 percentiles, whiskers at 10 and 90 percentiles, a dot
698 indicating the mean, and a line indicating the median. In Figure 3, mEPSC amplitudes were
699 measured within the same cell before and after NASPM application, so a paired t test was used
700 to compare the pre- and post-NASPM mEPSC amplitudes. In Figure 5A-C the mean mEPSC
701 amplitude for untreated and TTX-treated coverslips in the same culture are compared with a
702 paired t test. Statistics were computed and plots were created using Origin2020 (OriginLab).
703
704

705

706 References

707

708 Araki Y, Lin DT, Huganir RL (2010) Plasma membrane insertion of the AMPA receptor GluA2 subunit is
709 regulated by NSF binding and Q/R editing of the ion pore. Proc Natl Acad Sci U S A 107:11080-
710 11085.
711 Beattie EC, Stellwagen D, Morishita W, Bresnahan JC, Ha BK, Von Zastrow M, Beattie MS, Malenka RC
712 (2002) Control of synaptic strength by glial TNFalpha. Science 295:2282-2285.
713 Blaschke M, Keller BU, Rivosecchi R, Hollmann M, Heinemann S, Konnerth A (1993) A single amino acid
714 determines the subunit-specific spider toxin block of alpha-amino-3-hydroxy-5-methylisoxazole-
715 4-propionate/kainate receptor channels. Proc Natl Acad Sci U S A 90:6528-6532.
716 Bochet P, Audinat E, Lambolez B, Crepel F, Rossier J, Iino M, Tsuzuki K, Ozawa S (1994) Subunit
717 composition at the single-cell level explains functional properties of a glutamate-gated channel.
718 Neuron 12:383-388.
719 Burnashev N, Monyer H, Seeburg PH, Sakmann B (1992) Divalent ion permeability of AMPA receptor
720 channels is dominated by the edited form of a single subunit. Neuron 8:189-198.
721 Castillo PE, Janz R, Sudhof TC, Tzounopoulos T, Malenka RC, Nicoll RA (1997) Rab3A is essential for
722 mossy fibre long-term potentiation in the hippocampus. Nature 388:590-593.
723 Chang CW, Chiang CW, Jackson MB (2017) Fusion pores and their control of neurotransmitter and
724 hormone release. J Gen Physiol 149:301-322.
725 Cheresharov L, Ovtscharoff W, Manolov S (1978) Ultrastructural changes in the anterior horn synapses
726 of rat spinal cord under different locomotor conditions. J Neural Transm 42:9-21.
727 Chiang CW, Chang CW, Jackson MB (2018) The Transmembrane Domain of Synaptobrevin Influences
728 Neurotransmitter Flux through Synaptic Fusion Pores. J Neurosci 38:7179-7191.
729 Coleman WL, Bykhovskaia M (2009) Rab3a-mediated vesicle recruitment regulates short-term plasticity
730 at the mouse diaphragm synapse. Mol Cell Neurosci 41:286-296.
731 Coleman WL, Bykhovskaia M (2010) Cooperative regulation of neurotransmitter release by Rab3a and
732 synapsin II. Mol Cell Neurosci 44:190-200.
733 Coleman WL, Bill CA, Bykhovskaia M (2007) Rab3a deletion reduces vesicle docking and transmitter
734 release at the mouse diaphragm synapse. Neuroscience 148:1-6.
735 Daniels RW, Collins CA, Gelfand MV, Dant J, Brooks ES, Krantz DE, DiAntonio A (2004) Increased
736 expression of the Drosophila vesicular glutamate transporter leads to excess glutamate release
737 and a compensatory decrease in quantal content. J Neurosci 24:10466-10474.
738 De Gois S, Schafer MK, Defamie N, Chen C, Ricci A, Weihe E, Varoqui H, Erickson JD (2005) Homeostatic
739 scaling of vesicular glutamate and GABA transporter expression in rat neocortical circuits. J
740 Neurosci 25:7121-7133.
741 Diaz-Rohrer B, Castello-Serrano I, Chan SH, Wang HY, Shurer CR, Levental KR, Levental I (2023) Rab3
742 mediates a pathway for endocytic sorting and plasma membrane recycling of ordered
743 microdomains. Proc Natl Acad Sci U S A 120:e2207461120.
744 Diering GH, Nirujogi RS, Roth RH, Worley PF, Pandey A, Huganir RL (2017) Homer1a drives homeostatic
745 scaling-down of excitatory synapses during sleep. Science 355:511-515.
746 Dubes S, Soula A, Benquet S, Tessier B, Poujol C, Favereaux A, Thoumine O, Letellier M (2022) miR-124-
747 dependent tagging of synapses by synaptopodin enables input-specific homeostatic plasticity.
748 EMBO J 41:e109012.

749 Fan D, Grooms SY, Araneda RC, Johnson AB, Dobrenis K, Kessler JA, Zukin RS (1999) AMPA receptor
750 protein expression and function in astrocytes cultured from hippocampus. J Neurosci Res
751 57:557-571.
752 Fernandes D, Carvalho AL (2016) Mechanisms of homeostatic plasticity in the excitatory synapse. J
753 Neurochem 139:973-996.
754 Geppert M, Bolshakov VY, Siegelbaum SA, Takei K, De Camilli P, Hammer RE, Sudhof TC (1994) The role
755 of Rab3A in neurotransmitter release. Nature 369:493-497.
756 Gu Y, Chiu SL, Liu B, Wu PH, Delannoy M, Lin DT, Wirtz D, Huganir RL (2016) Differential vesicular sorting
757 of AMPA and GABAA receptors. Proc Natl Acad Sci U S A 113:E922-931.
758 Hanes AL, Koesters AG, Fong MF, Altimimi HF, Stellwagen D, Wenner P, Engisch KL (2020) Divergent
759 Synaptic Scaling of Miniature EPSCs following Activity Blockade in Dissociated Neuronal Cultures.
760 J Neurosci 40:4090-4102.
761 Hartman KN, Pal SK, Burrone J, Murthy VN (2006) Activity-dependent regulation of inhibitory synaptic
762 transmission in hippocampal neurons. Nat Neurosci 9:642-649.
763 Heir R, Abbasi Z, Komal P, Altimimi HF, Franquin M, Moschou D, Chambon J, Stellwagen D (2024)
764 Astrocytes Are the Source of TNF Mediating Homeostatic Synaptic Plasticity. J Neurosci 44.
765 Herlitze S, Raditsch M, Ruppersberg JP, Jahn W, Monyer H, Schoepfer R, Witzemann V (1993) Argiotoxin
766 detects molecular differences in AMPA receptor channels. Neuron 10:1131-1140.
767 Hollmann M, Hartley M, Heinemann S (1991) Ca2+ permeability of KA-AMPA--gated glutamate receptor
768 channels depends on subunit composition. Science 252:851-853.
769 Hong Y, Zhao T, Li XJ, Li S (2016) Mutant Huntingtin Impairs BDNF Release from Astrocytes by Disrupting
770 Conversion of Rab3a-GTP into Rab3a-GDP. J Neurosci 36:8790-8801.
771 Hou Q, Zhang D, Jarzylo L, Huganir RL, Man HY (2008) Homeostatic regulation of AMPA receptor
772 expression at single hippocampal synapses. Proc Natl Acad Sci U S A 105:775-780.
773 Hu JH, Park JM, Park S, Xiao B, Dehoff MH, Kim S, Hayashi T, Schwarz MK, Huganir RL, Seeburg PH,
774 Linden DJ, Worley PF (2010) Homeostatic scaling requires group I mGluR activation mediated by
775 Homer1a. Neuron 68:1128-1142.
776 Hussain S, Davanger S (2015) Postsynaptic VAMP/Synaptobrevin Facilitates Differential Vesicle
777 Trafficking of GluA1 and GluA2 AMPA Receptor Subunits. PLoS One 10:e0140868.
778 Ibata K, Sun Q, Turrigiano GG (2008) Rapid synaptic scaling induced by changes in postsynaptic firing.
779 Neuron 57:819-826.
780 Iino M, Koike M, Isa T, Ozawa S (1996) Voltage-dependent blockage of Ca(2+)-permeable AMPA
781 receptors by joro spider toxin in cultured rat hippocampal neurones. J Physiol 496 (Pt 2):431-
782 437.
783 Jakawich SK, Neely RM, Djakovic SN, Patrick GN, Sutton MA (2010) An essential postsynaptic role for the
784 ubiquitin proteasome system in slow homeostatic synaptic plasticity in cultured hippocampal
785 neurons. Neuroscience 171:1016-1031.
786 Jonas P, Burnashev N (1995) Molecular mechanisms controlling calcium entry through AMPA-type
787 glutamate receptor channels. Neuron 15:987-990.
788 Ju W, Morishita W, Tsui J, Gaietta G, Deerinck TJ, Adams SR, Garner CC, Tsien RY, Ellisman MH, Malenka
789 RC (2004) Activity-dependent regulation of dendritic synthesis and trafficking of AMPA
790 receptors. Nat Neurosci 7:244-253.
791 Jurado S, Goswami D, Zhang Y, Molina AJ, Sudhof TC, Malenka RC (2013) LTP requires a unique
792 postsynaptic SNARE fusion machinery. Neuron 77:542-558.
793 Kapfhamer D, Valladares O, Sun Y, Nolan PM, Rux JJ, Arnold SE, Veasey SC, Bucan M (2002) Mutations in
794 Rab3a alter circadian period and homeostatic response to sleep loss in the mouse. Nat Genet
795 32:290-295.

796 Karunanithi S, Marin L, Wong K, Atwood HL (2002) Quantal size and variation determined by vesicle size
797 in normal and mutant Drosophila glutamatergic synapses. J Neurosci 22:10267-10276.
798 Kavalali ET, Monteggia LM (2023) Rapid homeostatic plasticity and neuropsychiatric therapeutics.
799 Neuropsychopharmacology 48:54-60.
800 Kawana E, Akert K, Bruppacher H (1971) Enlargement of synaptic vesicles as an early sign of terminal
801 degneration in the rat caudate nucleus. J Comp Neurol 142:297-307.
802 Kennedy MJ, Davison IG, Robinson CG, Ehlers MD (2010) Syntaxin-4 defines a domain for activity-
803 dependent exocytosis in dendritic spines. Cell 141:524-535.
804 Koesters AG, Rich MM, Engisch KL (2024) Diverging from the Norm: Reevaluating What Miniature
805 Excitatory Postsynaptic Currents Tell Us about Homeostatic Synaptic Plasticity. Neuroscientist
806 30:49-70.
807 Koike M, Iino M, Ozawa S (1997) Blocking effect of 1-naphthyl acetyl spermine on Ca(2+)-permeable
808 AMPA receptors in cultured rat hippocampal neurons. Neurosci Res 29:27-36.
809 Leenders AG, Lopes da Silva FH, Ghijsen WE, Verhage M (2001) Rab3a is involved in transport of synaptic
810 vesicles to the active zone in mouse brain nerve terminals. Mol Biol Cell 12:3095-3102.
811 Lignani G, Baldelli P, Marra V (2020) Homeostatic Plasticity in Epilepsy. Front Cell Neurosci 14:197.
812 Lledo PM, Zhang X, Sudhof TC, Malenka RC, Nicoll RA (1998) Postsynaptic membrane fusion and long-
813 term potentiation. Science 279:399-403.
814 Lloret IL, Saavedra JP (1975) Enlargement of synaptic vesicles in degenerating nerve endings: a
815 comparison between cat and monkey. J Neurocytol 4:1-6.
816 Lonart G, Janz R, Johnson KM, Sudhof TC (1998) Mechanism of action of rab3A in mossy fiber LTP.
817 Neuron 21:1141-1150.
818 Lovinger DM, Abrahao KP (2018) Synaptic plasticity mechanisms common to learning and alcohol use
819 disorder. Learn Mem 25:425-434.
820 Maienschein V, Marxen M, Volknandt W, Zimmermann H (1999) A plethora of presynaptic proteins
821 associated with ATP-storing organelles in cultured astrocytes. Glia 26:233-244.
822 Mansour M, Nagarajan N, Nehring RB, Clements JD, Rosenmund C (2001) Heteromeric AMPA receptors
823 assemble with a preferred subunit stoichiometry and spatial arrangement. Neuron 32:841-853.
824 Nishimune A, Isaac JT, Molnar E, Noel J, Nash SR, Tagaya M, Collingridge GL, Nakanishi S, Henley JM
825 (1998) NSF binding to GluR2 regulates synaptic transmission. Neuron 21:87-97.
826 O'Brien RJ, Kamboj S, Ehlers MD, Rosen KR, Fischbach GD, Huganir RL (1998) Activity-dependent
827 modulation of synaptic AMPA receptor accumulation. Neuron 21:1067-1078.
828 Ormel L, Stensrud MJ, Bergersen LH, Gundersen V (2012) VGLUT1 is localized in astrocytic processes in
829 several brain regions. Glia 60:229-238.
830 Osten P, Srivastava S, Inman GJ, Vilim FS, Khatri L, Lee LM, States BA, Einheber S, Milner TA, Hanson PI,
831 Ziff EB (1998) The AMPA receptor GluR2 C terminus can mediate a reversible, ATP-dependent
832 interaction with NSF and alpha- and beta-SNAPs. Neuron 21:99-110.
833 Pozo K, Goda Y (2010) Unraveling mechanisms of homeostatic synaptic plasticity. Neuron 66:337-351.
834 Riedel D, Antonin W, Fernandez-Chacon R, Alvarez de Toledo G, Jo T, Geppert M, Valentijn JA, Valentijn
835 K, Jamieson JD, Sudhof TC, Jahn R (2002) Rab3D is not required for exocrine exocytosis but for
836 maintenance of normally sized secretory granules. Mol Cell Biol 22:6487-6497.
837 Sanderson JL, Scott JD, Dell'Acqua ML (2018) Control of Homeostatic Synaptic Plasticity by AKAP-
838 Anchored Kinase and Phosphatase Regulation of Ca(2+)-Permeable AMPA Receptors. J Neurosci
839 38:2863-2876.
840 Schluter OM, Basu J, Sudhof TC, Rosenmund C (2006) Rab3 superprimes synaptic vesicles for release:
841 implications for short-term synaptic plasticity. J Neurosci 26:1239-1246.

842 Schonn JS, van Weering JR, Mohrmann R, Schluter OM, Sudhof TC, de Wit H, Verhage M, Sorensen JB
843 (2010) Rab3 proteins involved in vesicle biogenesis and priming in embryonic mouse chromaffin
844 cells. Traffic 11:1415-1428.
845 Shepherd JD, Rumbaugh G, Wu J, Chowdhury S, Plath N, Kuhl D, Huganir RL, Worley PF (2006)
846 Arc/Arg3.1 mediates homeostatic synaptic scaling of AMPA receptors. Neuron 52:475-484.
847 Silva MM, Rodrigues B, Fernandes J, Santos SD, Carreto L, Santos MAS, Pinheiro P, Carvalho AL (2019)
848 MicroRNA-186-5p controls GluA2 surface expression and synaptic scaling in hippocampal
849 neurons. Proc Natl Acad Sci U S A 116:5727-5736.
850 Smith-Dijak AI, Nassrallah WB, Zhang LYJ, Geva M, Hayden MR, Raymond LA (2019) Impairment and
851 Restoration of Homeostatic Plasticity in Cultured Cortical Neurons From a Mouse Model of
852 Huntington Disease. Front Cell Neurosci 13:209.
853 Song I, Kamboj S, Xia J, Dong H, Liao D, Huganir RL (1998) Interaction of the N-ethylmaleimide-sensitive
854 factor with AMPA receptors. Neuron 21:393-400.
855 Stellwagen D, Malenka RC (2006) Synaptic scaling mediated by glial TNF-alpha. Nature 440:1054-1059.
856 Stellwagen D, Beattie EC, Seo JY, Malenka RC (2005) Differential regulation of AMPA receptor and GABA
857 receptor trafficking by tumor necrosis factor-alpha. J Neurosci 25:3219-3228.
858 Suh YH, Terashima A, Petralia RS, Wenthold RJ, Isaac JT, Roche KW, Roche PA (2010) A neuronal role for
859 SNAP-23 in postsynaptic glutamate receptor trafficking. Nat Neurosci 13:338-343.
860 Sun HY, Bartley AF, Dobrunz LE (2009) Calcium-permeable presynaptic kainate receptors involved in
861 excitatory short-term facilitation onto somatostatin interneurons during natural stimulus
862 patterns. J Neurophysiol 101:1043-1055.
863 Sutton MA, Ito HT, Cressy P, Kempf C, Woo JC, Schuman EM (2006) Miniature neurotransmission
864 stabilizes synaptic function via tonic suppression of local dendritic protein synthesis. Cell
865 125:785-799.
866 Suzuki K, Kim JW, Nosyreva E, Kavalali ET, Monteggia LM (2021) Convergence of distinct signaling
867 pathways on synaptic scaling to trigger rapid antidepressant action. Cell Rep 37:109918.
868 Swanson GT, Kamboj SK, Cull-Candy SG (1997) Single-channel properties of recombinant AMPA
869 receptors depend on RNA editing, splice variation, and subunit composition. J Neurosci 17:58-
870 69.
871 Tatavarty V, Sun Q, Turrigiano GG (2013) How to scale down postsynaptic strength. J Neurosci 33:13179-
872 13189.
873 Thiagarajan TC, Lindskog M, Tsien RW (2005) Adaptation to synaptic inactivity in hippocampal neurons.
874 Neuron 47:725-737.
875 Tian M, Xu CS, Montpetit R, Kramer RH (2012) Rab3A mediates vesicle delivery at photoreceptor ribbon
876 synapses. J Neurosci 32:6931-6936.
877 Tononi G, Cirelli C (2014) Sleep and the price of plasticity: from synaptic and cellular homeostasis to
878 memory consolidation and integration. Neuron 81:12-34.
879 Torrado Pacheco A, Bottorff J, Gao Y, Turrigiano GG (2021) Sleep Promotes Downward Firing Rate
880 Homeostasis. Neuron 109:530-544 e536.
881 Trasande CA, Ramirez JM (2007) Activity deprivation leads to seizures in hippocampal slice cultures: is
882 epilepsy the consequence of homeostatic plasticity? J Clin Neurophysiol 24:154-164.
883 Turrigiano GG, Nelson SB (2004) Homeostatic plasticity in the developing nervous system. Nat Rev
884 Neurosci 5:97-107.
885 Turrigiano GG, Leslie KR, Desai NS, Rutherford LC, Nelson SB (1998) Activity-dependent scaling of
886 quantal amplitude in neocortical neurons. Nature 391:892-896.
887 Wang G, Zhong J, Guttieres D, Man HY (2019) Non-scaling regulation of AMPA receptors in homeostatic
888 synaptic plasticity. Neuropharmacology 158:107700.

889 Wang JKT, Langfelder P, Horvath S, Palazzolo MJ (2017) Exosomes and Homeostatic Synaptic Plasticity
890 Are Linked to Each other and to Huntington's, Parkinson's, and Other Neurodegenerative
891 Diseases by Database-Enabled Analyses of Comprehensively Curated Datasets. Front Neurosci
892 11:149.
893 Wang X, Thiagarajan R, Wang Q, Tewolde T, Rich MM, Engisch KL (2008) Regulation of quantal shape by
894 Rab3A: evidence for a fusion pore-dependent mechanism. J Physiol 586:3949-3962.
895 Wang X, Wang Q, Yang S, Bucan M, Rich MM, Engisch KL (2011) Impaired activity-dependent plasticity of
896 quantal amplitude at the neuromuscular junction of Rab3A deletion and Rab3A earlybird mutant
897 mice. J Neurosci 31:3580-3588.
898 Wang X, Li Y, Engisch KL, Nakanishi ST, Dodson SE, Miller GW, Cope TC, Pinter MJ, Rich MM (2005)
899 Activity-dependent presynaptic regulation of quantal size at the mammalian neuromuscular
900 junction in vivo. J Neurosci 25:343-351.
901 Watt AJ, van Rossum MC, MacLeod KM, Nelson SB, Turrigiano GG (2000) Activity coregulates quantal
902 AMPA and NMDA currents at neocortical synapses. Neuron 26:659-670.
903 Weisskopf MG, Castillo PE, Zalutsky RA, Nicoll RA (1994) Mediation of hippocampal mossy fiber long-
904 term potentiation by cyclic AMP. Science 265:1878-1882.
905 Wierenga CJ, Ibata K, Turrigiano GG (2005) Postsynaptic expression of homeostatic plasticity at
906 neocortical synapses. J Neurosci 25:2895-2905.
907 Wilson NR, Kang J, Hueske EV, Leung T, Varoqui H, Murnick JG, Erickson JD, Liu G (2005) Presynaptic
908 regulation of quantal size by the vesicular glutamate transporter VGLUT1. J Neurosci 25:6221-
909 6234.
910 Wu D, Bacaj T, Morishita W, Goswami D, Arendt KL, Xu W, Chen L, Malenka RC, Sudhof TC (2017)
911 Postsynaptic synaptotagmins mediate AMPA receptor exocytosis during LTP. Nature 544:316-
912 321.
913 Xu X, Pozzo-Miller L (2017) EEA1 restores homeostatic synaptic plasticity in hippocampal neurons from
914 Rett syndrome mice. J Physiol 595:5699-5712.

915

Table 1. Comparison of mEPSC amplitude and GluA2 receptor cluster characteristics in mouse cortical cultures prepared from Rab3A$^{+/+}$ mice, and Rab3A$^{-/-}$ mice. *, $p < 0.05$, Kruskal-Wallis test.

	Rab3A$^{+/+}$				**Rab3A$^{-/-}$**			
Quantity	**CON Mean, SE**	**TTX Mean, SE (N, cultures)**	**% change**	**p value**	**CON Mean, SE (N, cultures)**	**TTX Mean, SE (N, cultures)**	**% change**	**p value**
mEPSC amplitude	13.7 ± 0.9 pA (23 cells, 3 cultures)	16.4 ± 0.9 pA (24 cells, 3 cultures)	+19.7	*p = 0.02	14.9 ± 0.8 pA (21 cells, 3 cultures)	13.5 ± 0.9 pA (21 cells, 3 cultures)	-9.4	p = 0.18
GluA2 cluster size	0.83 ± 0.04 μm^2 (49 cells, 5 cultures)	0.98 ± 0.07 μm^2 (48 cells, 5 cultures)	+18.1	p = 0.21	0.93 ± 0.05 μm^2 (30 cells, 3 cultures)	0.91 ± 0.05 μm^2 (29 cells, 3 cultures)	-2.2	p = 0.75
GluA2 cluster intensity	733 ± 14 a.u. (49 cells, 5 cultures)	738 ± 13 a.u. (48 cells, 5 cultures)	+0.7	p = 0.69	766 ± 12 a.u. (30 cells, 3 cultures)	776 ± 15 a.u. (29 cells, 3 cultures)	+1.3	p = 0.46
GluA2 cluster integral	311021 ± 19282 a.u. (49 cells, 5 cultures)	365366 ± 27080 a.u. (48 cells, 5 cultures)	+17.4	p = 0.22	369436 ± 23439 a.u. (30 cells, 3 cultures)	364237 ± 25833 a.u. (29 cells, 3 cultures)	-0.8	p = 0.86

Table 2. Comparison of mEPSC amplitude and VGLUT1 positive presynaptic site characteristics in mouse cortical cultures prepared from Rab3A$^{+/+}$ and Rab3A$^{-/-}$ mice. mEPSC data are identical to that in Table 1, reproduced here for comparison purposes. *, $p < 0.05$, Kruskal-Wallis test.

	Rab3A$^{+/+}$				**Rab3A$^{-/-}$**			
Quantity	**CON Mean, SE**	**TTX Mean, SE**	**% change**	**p value**	**CON Mean, SE**	**TTX Mean, SE**	**% change**	**p value**
mEPSC amplitude	13.7 ± 0.9 pA (23 cells, 3 cultures)	16.4 ± 0.9 pA (24 cells, 3 cultures)	+19.7	*p = 0.02	14.9 ± 0.8 pA (21 cells, 3 cultures)	13.5 ± 0.9 pA (21 cells, 3 cultures)	-9.4	p = 0.18
VGLUT1 site size	1.17 ± 0.08 μm^2 (29 cells, 3 cultures)	1.07 ± 0.06 μm^2 (24 cells, 3 cultures)	-7.7	p = 0.97	0.89 ± 0.03 μm^2 (30 cells, 3 cultures)	0.95 ± 0.04 μm^2 (29 cells, 3 cultures)	+6.7	p = 0.55
VGLUT1 site intensity	699 ± 39 a.u. (29 cells, 3 cultures)	639 ± 31 a.u. (28 cells, 3 cultures)	-8.6	p = 0.28	554 ± 13 a.u. (30 cells, 3 cultures)	570 ± 19 a.u. (29 cells, 3 cultures)	+2.9	p = 0.18
VGLUT1 site integral	430787 ± 36818 a.u. (29 cells, 3 cultures)	351653 ± 21689 a.u. (28 cells, 3 cultures)	-18.4	p = 0.13	257159 ± 18265 a.u. (30 cells, 3 cultures)	289857 ± 18521 a.u. (29 cells, 3 cultures)	+12.7	p = 0.21

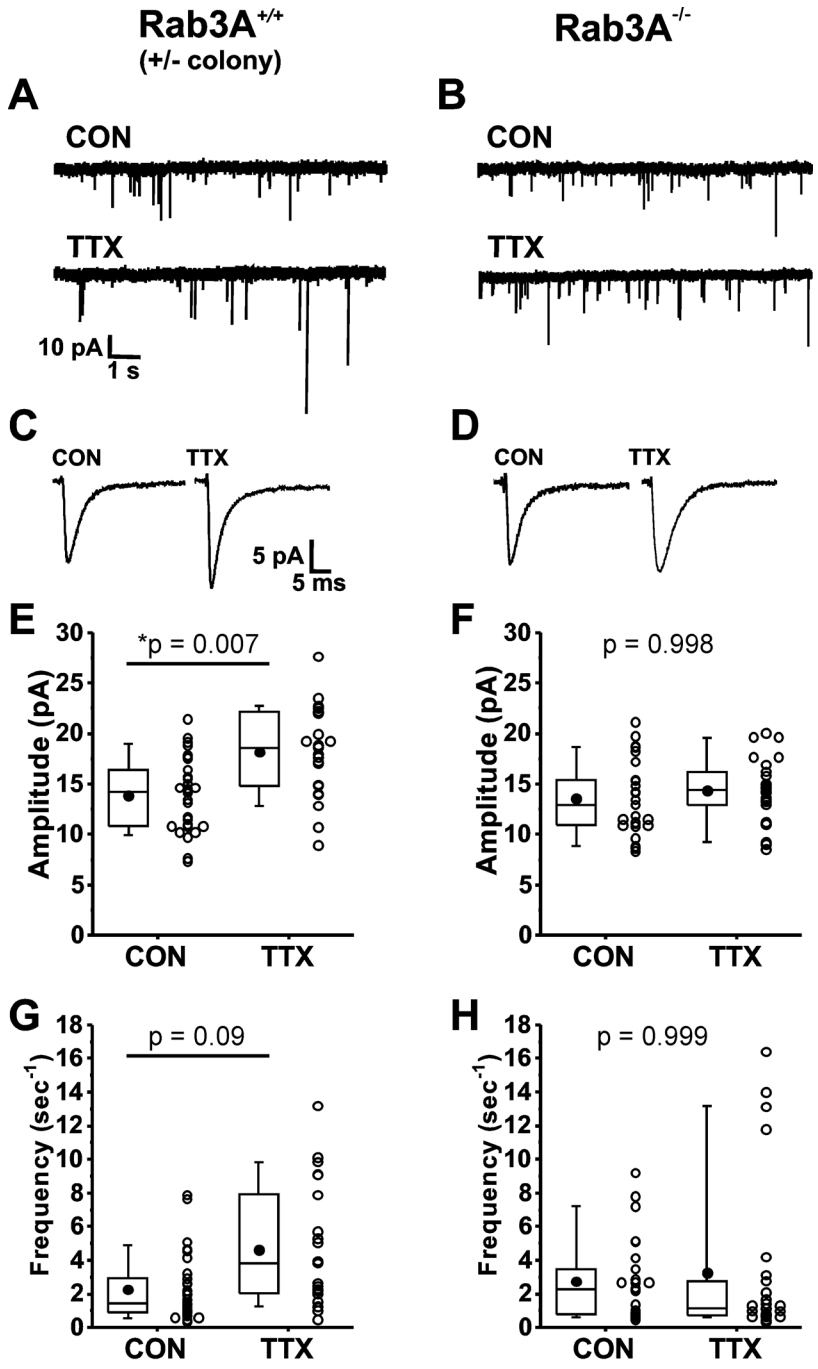

Figure 1. Loss of Rab3A disrupted the TTX-induced increase in amplitudes of mEPSCs recorded in cultured mouse cortical neurons; the increase in frequency was more variable but also appears to be reduced.

(A) Ten second example traces recorded at -60 mV in pyramidal cortical neurons from an untreated ("CON") and TTX-treated ("TTX") neuron in cultures prepared from Rab3A$^{+/+}$ mice

from the Rab3A$^{+/-}$ colony. (B) Ten second example traces recorded at -60 mV in pyramidal cortical neurons from an untreated ("CON") and TTX-treated ("TTX") neuron in cultures prepared from Rab3A$^{-/-}$ mice. (C & D) Average traces for the recordings shown in A and B, respectively. (E) Box plots for average mEPSC amplitudes from untreated cells and TTX-treated cells in cultures prepared from Rab3A$^{+/+}$ mice (Rab3A$^{+/-}$ colony; CON, N = 30 cells, 13.9 ± 0.7 pA; TTX, N = 23 cells, 18.2 ± 0.9 pA; from 11 cultures). (F) Box plots for average mEPSC amplitudes from untreated cells and TTX-treated cells in cultures prepared from Rab3A$^{-/-}$ mice (CON, N = 25 cells, 13.6 ± 0.7 pA; TTX, N = 26 cells, 14.3 ± 0.6 pA); from 11 cultures. (G) Box plots for average mEPSC frequency for same Rab3A$^{+/+}$ cells as in (E) (CON, 2.26 ± 0.37 sec^{-1}; TTX, 4.62 ± 0.74 sec^{-1}). (H) Box plots for average mEPSC frequency for same Rab3A$^{-/-}$cells as in (F) (CON, 2.74 ± 0.49 sec^{-1}; TTX, 3.23 ± 0.93 sec^{-1}). Box plot parameters: box ends, 25th and 75th percentiles; whiskers, 10th and 90th percentiles; open circles represent means from individual cells, bin size 0.1 pA, 0.5 sec^{-1}; line, median; dot, mean. p values (shown on the graphs) are from Tukey's post-hoc test following a two-way ANOVA. For all p-values, * with underline indicates significance with $p < 0.05$.

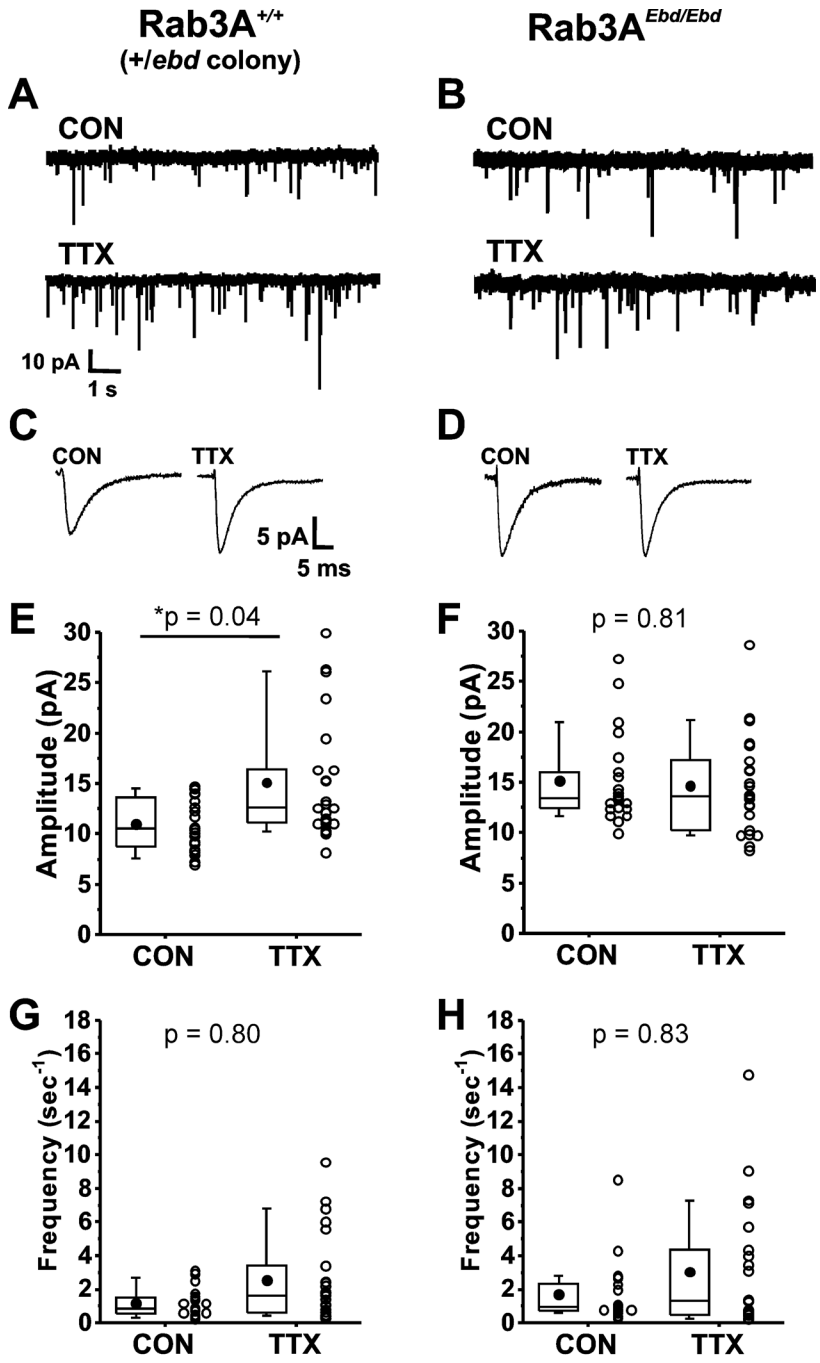

Figure 2. Normally functioning Rab3A was required for TTX-induced homeostatic plasticity of mEPSC amplitudes in cultured mouse cortical neurons.

(A) Ten second example traces recorded at -60 mV in pyramidal cortical neurons from an untreated ("CON") and TTX-treated ("TTX") neuron in cultures prepared from Rab3A$^{+/+}$ mice from the Rab3A$^{+/Ebd}$ colony. (B) Ten second example traces recorded at -60 mV in pyramidal cortical neurons from an untreated ("CON") and TTX-treated ("TTX") neuron in cultures

prepared from Rab3A$^{Ebd/Ebd}$ mice. (C & D) Average traces for the recordings shown in A and B, respectively. (E) Box plots for average mEPSC amplitudes from untreated cells and TTX-treated cells from cultures prepared from Rab3A$^{+/+}$ mice (Rab3A$^{+/Ebd}$ colony; CON, N = 20 cells, 11.0 ± 0.6 pA; TTX, N = 23 cells, 15.1 ± 1.2 pA; from 6 cultures). (F) Box plots for average mEPSC amplitudes from untreated cells and TTX-treated cells from cultures prepared from Rab3A$^{Ebd/Ebd}$ mice (CON, N = 21 cells, 15.1 ± 1.0 pA; TTX, N = 22 cells, 14.6 ± 1.1 pA; from 7 cultures.) (G) Box plots for average mEPSC frequency for same Rab3A$^{+/+}$ cells as in (E) (CON, 1.15 ± 0.19 sec^{-1}; TTX, 2.54 ± 0.55 sec^{-1}). (H) Box plots for average mEPSC frequency for same Rab3A$^{Ebd/Ebd}$ cells as in (F) (CON, 1.71 ± 0.41 sec^{-1}; TTX, 3.05 ± 0.80 sec^{-1}). Box plot parameters: box ends, 25th and 75th percentiles; whiskers, 10th and 90th percentiles; open circles represent means from individual cells; bin size 0.1 pA, 0.5 sec^{-1}; line, median; dot, mean. p values (shown on the graphs) are from a Tukey's post-hoc test following a two-way ANOVA. For all p-values, * with underline indicates significance with $p < 0.05$.

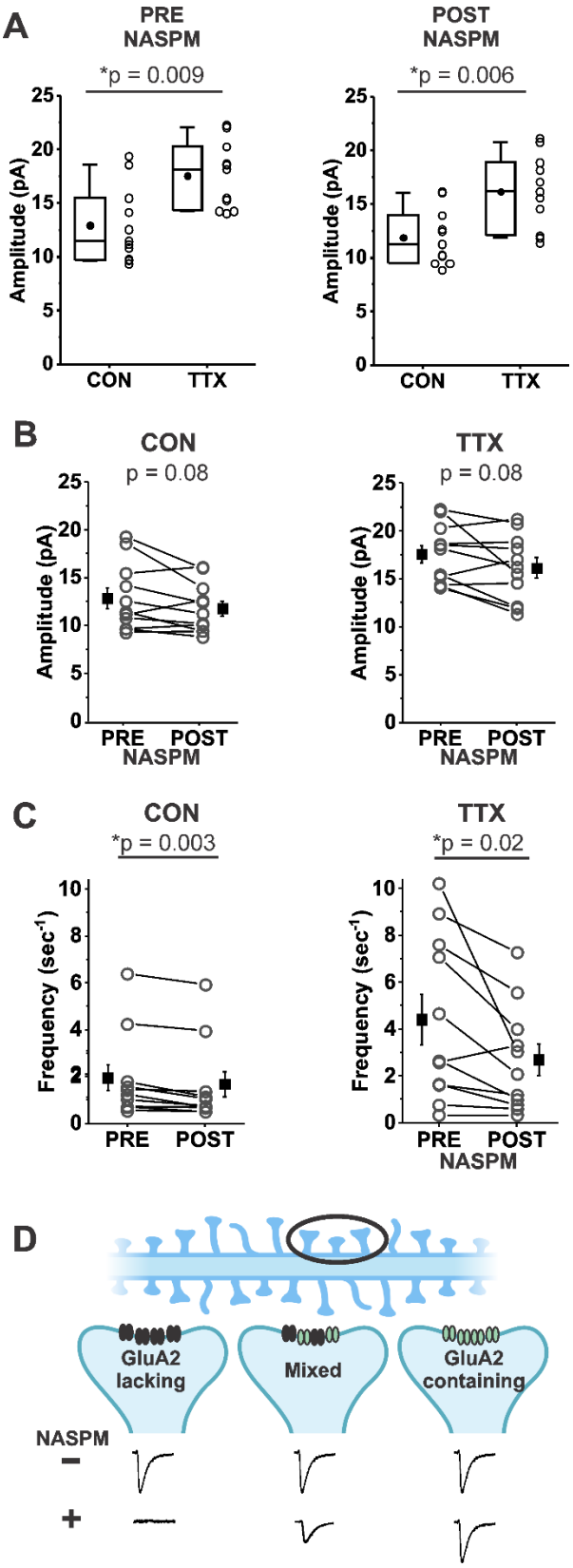
A
PRE NASPM
*p = 0.009
POST NASPM
*p = 0.006
Amplitude (pA)
CON
TTX
B
CON
p = 0.08
TTX
p = 0.08
PRE
POST
NASPM
C
CON
*p = 0.003
TTX
*p = 0.02
Frequency (sec-1)
D
GluA2 lacking
Mixed
GluA2 containing
NASPM
−
+

Figure 3

Figure 3. Homeostatic plasticity of mEPSC amplitudes in mouse cortical cultures treated with TTX for 48 hr was unchanged by acute inhibition of Ca^{2+} permeable AMPA receptors by NASPM (20 μm).

(A) Box plot comparison of the TTX effect on mEPSC amplitudes in the same pyramidal neurons before and after application of 20 μM NASPM. (N = 11 cells from 3 cultures; Pre-NASPM, CON: 12.9 ± 1.1 pA; TTX: 17.5 ± 0.9 pA; post-NASPM, CON: 11.9 ± 0.8 pA; TTX: 16.1 ± 1.0 pA). (B) Line series plot of mEPSC amplitudes before and after acute perfusion with 20 μM NASPM for untreated and TTX-treated pyramidal neurons; same cells as in (A); CON, pre-NASPM: 12.9 ± 1.1 pA; post-NASPM: 11.9 ± 0.8 pA; TTX, pre-NASPM: 17.5 ± 0.9 pA; post-NASPM: 16.1 ± 0.1 pA. (C) Line series plot of mEPSC frequency before and after acute perfusion with 20 μM NASPM for untreated and TTX-treated pyramidal neurons; same cells as in (A); CON, pre-NAPSM: 1.84 ± 0.55 sec^{-1}; post-NASPM; 1.56 ± 0.53 sec^{-1}; TTX, pre-NASPM: 4.40 ± 1.06 sec^{-1}; post-NASPM, 2.68 ± 0.68 sec^{-1}. (D) A proposed mechanism for why NASPM had a robust effect on frequency without greatly affecting amplitude. A dendrite with spines (Top) is expanded on three postsynaptic sites (Middle) to show possible types of AMPA receptor distributions: Left, at a site comprised only of Ca^{2+}-permeable AMPA receptors (NASPM-sensitive, GluA2-lacking receptors (black)), NASPM would completely inhibit the mEPSC, causing a decrease in frequency to be measured in the overall population; Right, at a site comprised only of Ca^{2+}-impermeable AMPA receptors (NASPM-insensitive, GluA2-containing receptors (green)), NASPM would have no effect on mEPSC amplitude; Middle, at a site comprised of a mix of Ca^{2+}-permeable and Ca^{2+}-impermeable AMPA receptors, NASPM would partially inhibit the mEPSC. Diagram produced in BioRender.com (2024). Box plot parameters: box ends, 25th and 75th percentiles; whiskers, 10th and 90th percentiles; open circles represent means from individual cells; bin size 0.1 pA; line, median; dot, mean. p values (shown on the graphs) are from Kruskal-Wallis test. Line series plot p values are from student's paired t test. For all p-values, * with underline indicates significance with $p < 0.05$.

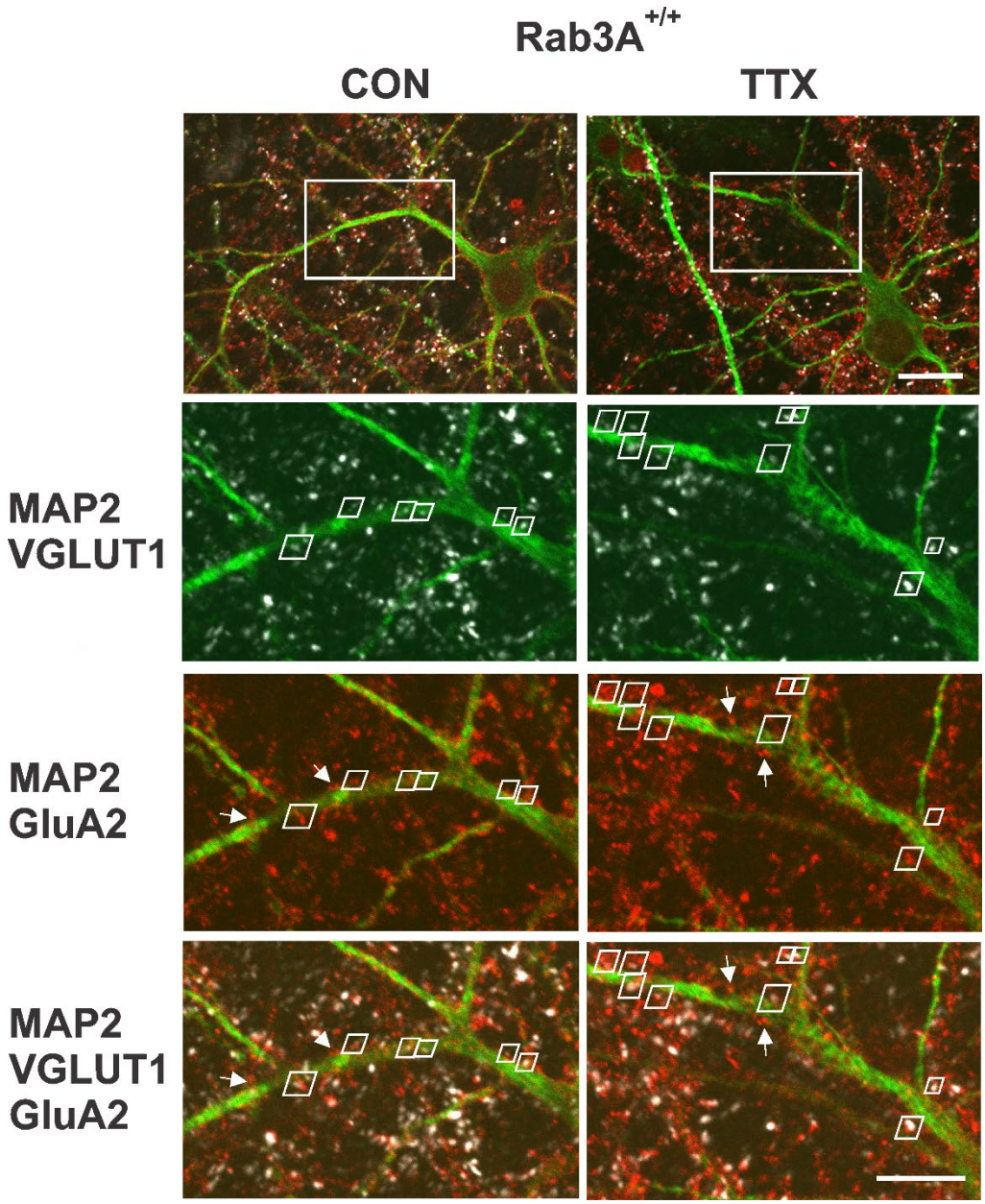

Figure 4. Identification of synaptic GluA2 receptor immunofluorescence on primary dendrites of pyramidal neurons in high density mouse cortical co-cultures prepared from Rab3A$^{+/+}$ mice.

(Top) Non-zoomed single confocal sections collected with a 60X oil immersion objective of recognizably pyramidal-shaped neurons, presumed to be excitatory neurons, selected for synaptic GluA2 analysis. A neuron was selected from an untreated coverslip (CON, Left) and a TTX-treated coverslip (TTX, Right) from the same culture prepared from Rab3A$^{+/+}$ animals (= Rab3A$^{+/+}$ Culture #2 in Figure 5). The white rectangular boxes indicate 5X zoomed areas shown in the images below. Note that the depth of the single confocal section of the non-zoomed neuron image is not at the same depth as the confocal section in zoomed dendritic image, so

some features are not visible in both images. Scale bar, 20 μm. (Bottom) 5X zoom single confocal sections selected for demonstration purposes because they had an unusually high number of identified synaptic pairs along the primary dendrite contained within a single confocal section. Synaptic pairs, highlighted with white trapezoids, were identified based on close proximity of GluA2 (red) and VGLUT1 (white) immunofluorescence, apposed to the MAP2 immunofluorescent primary dendrite (green). Some apparent synaptic pairs are not highlighted with a white trapezoid because there was a different confocal section in which the two immunofluorescent sites were maximally bright. There were GluA2 positive clusters located on the primary dendrites that were not apposed to VGLUT1-positive terminals (4 of these non-synaptic GluA2 clusters are highlighted with white arrows in the MAP2-GluA2 and MAP2-GluA2-VGLUT1 panels). Scale bar, 10 μm.

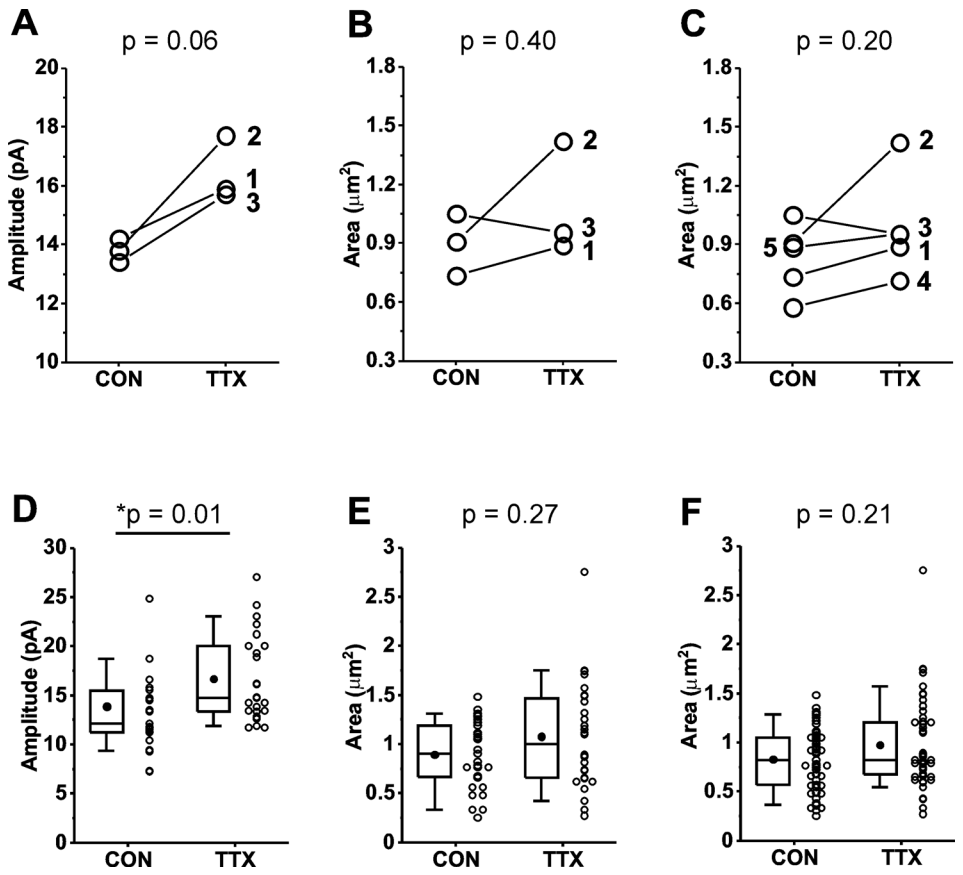

Figure 5. Comparison of mEPSC amplitudes and GluA2 receptor cluster areas in matched and unmatched mouse cortical cultures prepared from Rab3A$^{+/+}$ mice and treated with TTX for 48 hr.

(A) Culture averages of mEPSC amplitudes for untreated (CON) and TTX-treated coverslips (TTX) in each of 3 Rab3A$^{+/+}$ mouse cortical co-cultures. Culture #1, CON, N = 6, 14.2 $\pm$ 2.2 pA; TTX, N = 6, 15.9 $\pm$ 1.9 pA; Culture #2, CON, N = 7, 13.8 $\pm$ 2.4 pA; TTX, N = 8, 17.7 $\pm$ 1.8 pA; Culture #3, CON, N = 10, 13.4 $\pm$ 0.8 pA; TTX, N = 9, 15.7 $\pm$ 1.0 pA. (B) Culture averages of GluA2 receptor cluster size in the same 3 cultures as shown in (A). Culture #1, CON, N = 10, 0.73 $\pm$ 0.09 μm^2; TTX, N = 9, 0.89 $\pm$ 0.09 μm^2; Culture #2, CON, N = 9, 0.91 $\pm$ 0.12 μm^2; TTX, N = 9, 1.42 $\pm$ 0.24 μm^2; Culture #3, CON, N = 10, 1.05 $\pm$ 0.11 μm^2; TTX, N = 9, 0.95 $\pm$ 0.15 μm^2. (C) Two additional culture averages are included that did not have corresponding mEPSC recordings. Culture #4, CON, N = 10, 0.58 $\pm$ 0.07 μm^2: TTX, N = 10, 0.71 $\pm$ 0.04 μm^2; Culture 5, CON, N =10, 0.89 $\pm$ 0.05 μm^2; TTX, N = 10, 0.95 $\pm$ 0.08 μm^2. (D) Box plots of cell mean mEPSC amplitudes pooled from same 3 cultures as shown in (A). CON, N = 23 cells, 13.7 $\pm$ 0.9 pA; TTX, N = 24 cells, 16.4 $\pm$ 0.9 pA. (E) Box plots of dendrite mean GluA2 receptor cluster size pooled from same 3 cultures as shown in (A) and (B). CON, N = 29 dendrites, 0.90 $\pm$ 0.06 μm^2; TTX, N = 28 dendrites, 1.08 $\pm$ 0.10 μm^2. (F) Box plots of dendrite mean GluA2 receptor cluster size pooled from the same 5

cultures shown in (C). CON, N = 49 dendrites, 0.83 $\pm$ 0.04 μm^2; TTX, N = 48 dendrites, 0.98 $\pm$ 0.07 μm^2. Line series, Student's paired T test; box plots, Kruskal-Wallis test. Box plot parameters: box ends, 25th and 75th percentiles; whiskers, 10 and 90 percentiles; open circles indicate means of individual cells/dendrites; bin size 0.1 pA, 0.05 μm^2; line, median; dot, mean. For all p-values, * with underline indicates significance with $p < 0.05$.

.

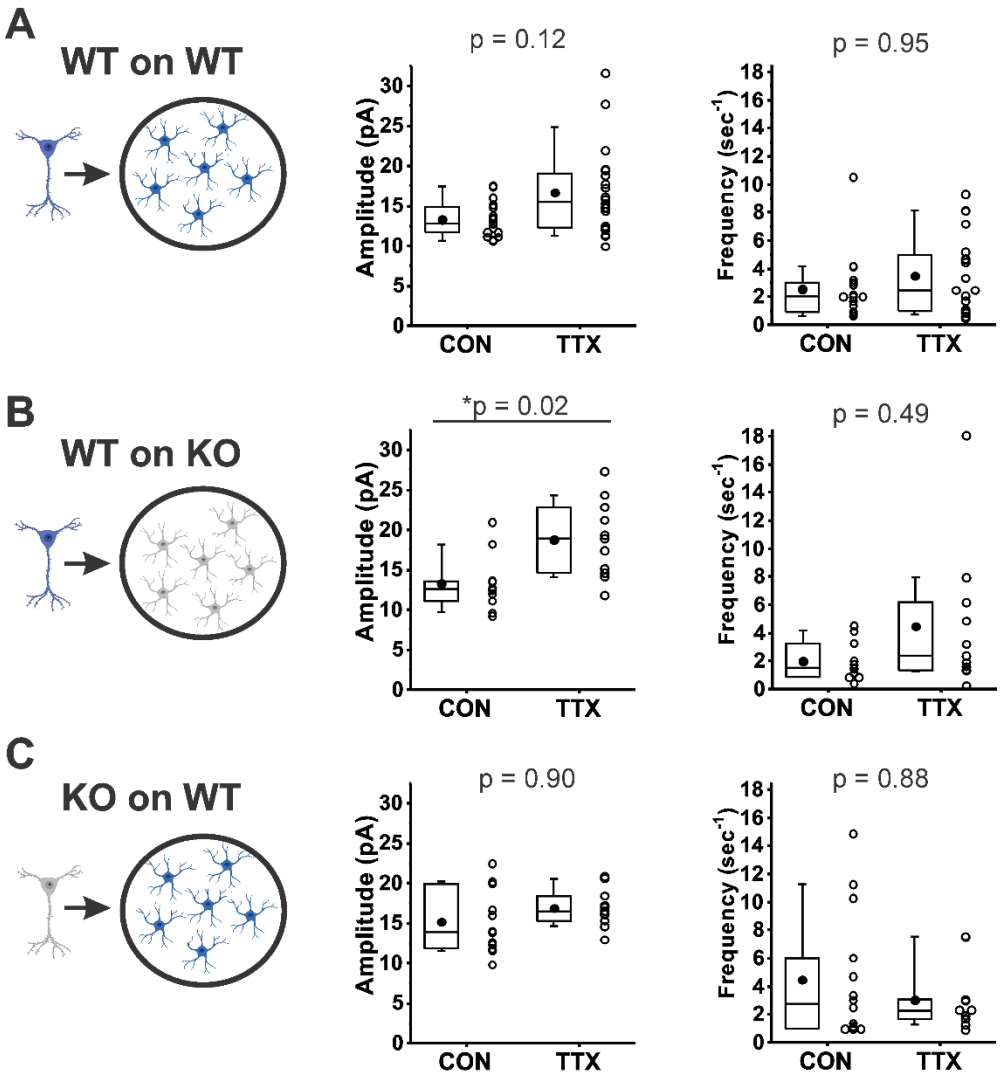

Figure 6. Rab3A in neurons, not astrocytes, was required for full TTX-induced homeostatic plasticity.

(A)-(C), mEPSC amplitude (Middle) and frequency (Right) data from dissociated cortical neurons plated on an astrocyte feeder layer, each prepared separately from the type of mice depicted in the schema (Left): (A) Neurons from Rab3A$^{+/+}$ mice plated on astrocytes from Rab3A$^{+/+}$ mice. Box plots for mEPSC amplitudes (CON, N = 17 cells, 13.3 ± 0.5 pA; TTX, N = 20 cells, 16.7 ± 1.2 pA) and mEPSC frequency in the same recordings (mean, CON, 2.54 ± 0.57 sec^{-1}; TTX, 3.48 ± 0.64 sec^{-1}); from 4 cultures. (B) Neurons from Rab3A$^{+/+}$ mice plated on astrocytes from Rab3A$^{-/-}$ mice. Box plots for average mEPSC amplitude (CON, N = 11 cells, 13.3 ± 1.0 pA; TTX, N = 11 cells,

18.8 ± 1.4 pA) and average mEPSC frequency in the same recordings (CON, 2.01 ± 0.41 sec^{-1}; TTX, 4.47 ± 1.53 sec^{-1}); from 2 cultures. (C) Neurons from $Rab3A^{-/-}$ neurons plated on astrocytes from $Rab3A^{+/+}$ mice. Box plots for average mEPSC amplitude (CON, N = 14 cells, 15.2 ± 1.1 pA; TTX, N = 11 cells, 16.9 ± 0.7 pA) and mEPSC frequency in the same recordings (CON, 4.47 ± 1.21 sec^{-1}; TTX, 3.02 ± 0.70 sec^{-1}); from 3 cultures. Box plot parameters: box ends, 25th and 75th percentiles; whiskers, 10th and 90th percentiles, bin size 0.1 pA; open circles represent means from individual cells; line, median; dot, mean. p values (shown on the graphs) are from Tukey's post-hoc test following a two-way ANOVA. p-values denoted with * and underline indicates significance of $p < 0.05$.

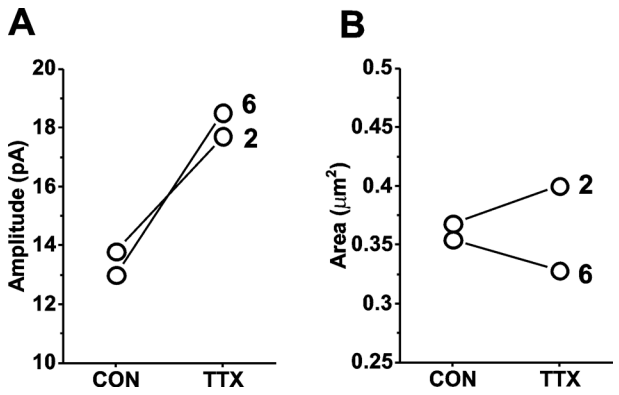

Supplemental Figure 1. Comparison of mEPSC amplitudes and GluA1 receptor cluster areas in matched mouse cortical cultures prepared from Rab3A$^{+/+}$ mice and treated with TTX for 48 hr.

(A) Culture averages of mEPSC amplitudes for untreated (CON) and TTX-treated coverslips (TTX) in each of 2 Rab3A$^{+/+}$ mouse cortical co-cultures. Culture #2, CON, N = 7, 13.8 $\pm$ 2.4 pA; TTX, N = 8, 17.7 $\pm$ 1.8 pA (+28.3%); Culture #6, CON, N = 6, 13.0 $\pm$ 1.5 pA; TTX, N = 6, 18.5 $\pm$ 2.0 pA (+42.3%). (B) Culture averages of GluA1 receptor cluster size in the same 2 cultures as shown in (A). Culture #2, CON, N = 10, 0.37 $\pm$ 0.04 μm^2; TTX, N = 10, 0.40 $\pm$ 0.06 μm^2 (+8.1%) Culture #6, CON, N = 10, 0.35 $\pm$ 0.05 μm^2; TTX, N = 10, 0.33 $\pm$ 0.04 μm^2 (-5.7%) "Culture #2" is the same Culture #2 depicted in Figure 5, different coverslips were processed for GluA1 immunofluorescence labeling. GluA1 receptor cluster intensity did not increase in Culture #2 (CON, 364 vs. TTX, 357) or Culture #6 (CON, 357 vs. TTX, 363). Live cultures were exposed to GluA1 antibody against the extracellular domain (ABN241, purchased from EMD Millipore, now available from Millipore Sigma) before being fixed and processed with secondary antibodies.